

Future Extreme Events in European Climate: An Exploration of Regional Climate Model Projections

Martin Beniston¹, David B. Stephenson², Ole B. Christensen³, Christopher A.T. Ferro²,
Christoph Frei⁴, Stéphane Goyette¹, Kirsten Halsnaes⁵, Tom Holt⁶, Kirsti Jylhä⁷,
Brigitte Koffi¹, Jean Palutikof⁶, Regina Schöll⁴, Tido Semmler⁸, Katja Woth⁹

- 1: Department of Geosciences, University of Fribourg, Switzerland
- 2: Department of Meteorology, University of Reading, United Kingdom
- 3: Danish Meteorological Institute, Copenhagen, Denmark
- 4: Swiss Federal Institute of Technology (ETH), Zurich, Switzerland
- 5: Risoe National Laboratory, Roskilde, Denmark
- 6: Climatic Research Unit, University of East Anglia, Norwich, United Kingdom
- 7: Finnish Meteorological Institute, Helsinki, Finland
- 8: Max-Planck-Institute for Meteorology, Hamburg, Germany
- 9: GKSS Research Center, Geesthacht, Germany

Abstract

This paper presents an overview of changes in the extreme events that are most likely to affect Europe in forthcoming decades. A variety of diagnostic methods are used to determine how heat waves, heavy precipitation, drought, wind storms, and storm surges change between present (1961-90) and future (2071-2100) regional climate model simulations produced by the PRUDENCE project. A summary of the main results follows.

Heat waves – Regional surface warming causes the frequency, intensity and duration of heat waves to increase over Europe. By the end of the 21st century, countries in central Europe will experience the same number of hot days as are currently experienced in southern Europe. The intensity of extreme temperatures increases more rapidly than the intensity of more moderate temperatures over the continental interior due to increases in temperature variability.

Precipitation – Heavy winter precipitation increases in central and northern Europe and decreases in the south; heavy summer precipitation increases in north-eastern Europe and decrease in the south. These changes reflect changes in mean precipitation. Mediterranean droughts start earlier in the year and last longer.

Winter storms – Extreme wind speeds increase between 45°N and 55°N, except over and south of the Alps, and become more north-westerly. These changes are associated with reductions in mean sea-level pressure and generate more North Sea storms, leading to increases in storm surge along the North Sea coast, especially in Holland, Germany and Denmark.

1. Introduction

Climate change is one of the greatest threats facing mankind in the 21st century. Surface temperatures are expected to continue to increase globally and major changes are likely to occur in the global hydrological and energy cycles (IPCC, 2001). The greatest threat to humans (and other components of terrestrial ecosystems) will be manifested locally via changes in regional extreme weather and climate events. European society, for example, is particularly vulnerable to changes in the frequency and intensity of extreme events such as heat waves, heavy precipitation, droughts, and wind storms.

Insurance statistics reveal that, after earthquakes, climate-related hazards take the heaviest toll on human life and generate some of the highest claims for insured damage (Figure 1, adapted from Munich Re, 2002). In the second half of the 20th century, earthquakes caused 71 ‘billion-dollar events’ globally but more than 170 events with similar costs were related to climatic extremes, in particular wind storms (tropical cyclones and mid-latitude winter storms), floods, droughts and heat-waves. Furthermore, there is evidence that insured losses from extreme climate events have increased in recent decades (Munich Re, 2002), due not only to increases in insured infrastructure – more cover, higher premiums (Swiss Re, 2003) – but also to recent changes in weather and climate extremes (e.g. more storms in the 1990s).

This paper presents an overview of changes in various high-risk events that are most likely to affect Europe in forthcoming decades. It aims to highlight some of the key findings from the extremes work undertaken as part of the European Union project PRUDENCE (Christensen *et al.*, 2002; <http://prudence.dmi.dk>). The PRUDENCE project aims to quantify the uncertainty originating from the choice of global and regional model formulation in climate-change downscaling experiments. Through a unique collaborative effort of nine European regional modeling groups, a coordinated set of climate modeling experiments has been conducted. The resulting large collection of model output makes it possible to examine the relative influence of emissions scenario, global model, and regional model on the spread of model results.

This paper focuses on heat waves, heavy precipitation events, droughts, winter storms, and storm sea surges because of their large impacts on Europe. A variety of diagnostic methods are applied to determine features of these events in present (1961-90) and future (2071-2100) simulations produced by PRUDENCE and, therefore, how the events are predicted to change by the end of the 21st century. Section 2 reviews the various methodologies used in this study to define and analyze extremes.

Section 3 briefly discusses the RCM model experiments. Section 4 presents the key results for heat waves, precipitation extremes, and wind storms/surges. Section 5 summarizes the main findings.

2. Definition of extreme events and methodology

The following three criteria are often used in climate science to classify events as extreme.

- Rare – Events that occur with relatively low frequency. For example, the IPCC (2001) defines an ‘extreme weather event’ to be ‘an event that is rare within its statistical reference distribution at a particular place. Definitions of “rare” vary, but an extreme weather event would normally be as rare or rarer than the 10th or 90th percentile.’
- Intense – Events characterized by relatively small or large values. Not all intense events are rare: for example, low precipitation totals are often far from the mean precipitation but can still occur quite frequently.
- Severe – Events that result in large socio-economic losses. Severity is a complex criterion because damaging impacts can occur in the absence of a rare or intense climatic event: for example, thawing of mountain permafrost leading to rock falls and mud-slides.

The exploratory analyses presented in Section 4 of this paper are designed to reveal how the simulated climate responds to changes in emissions and model formulation, and therefore focus on meteorological events that are either rare or intense, but not necessarily severe. Table 1 summarizes the extreme events to be considered, and contains three types: maxima, percentiles, and threshold-based indices. Seasonal or annual maxima, such as the summer maximum one-day precipitation totals analyzed in Section 4.2, are simple summaries of extremal behavior. The p th percentile of a data sample is the value below which approximately $p\%$ of the data fall. Attention can be focused on different parts of the probability density function (PDF), which summarizes the relative frequencies of the data values, by choosing different percentages p . Indices commonly summarize those data that exceed some threshold, such as the number of days per year on which the temperature at a particular location exceeds 30°C (Section 4.1). This index is based on an absolute threshold but a relative threshold, such as the 90th percentile of the daily maximum temperatures at that location, could be used instead. Adopting a single, absolute threshold for all locations is simple to understand and ensures that indices measure events of a fixed intensity; a single, relative threshold ensures that indices measure events of a fixed rarity.

Such a variety of complementary definitions is required to obtain a broad view of extreme events in the PRUDENCE simulations. A similarly wide range of techniques is required to analyze them and to assess differences between the extreme events in different simulations. The behavior of maxima can

be summarized during a particular period by sample statistics such as the mean (Sections 4.2d, 4.3d) and these support straightforward comparisons. Probability models, such as the generalized extreme-value distribution motivated from extreme-value theory (e.g. Kharin and Zwiers, 2000; Coles, 2001), can also be fitted to maxima to obtain a more complete description of their statistical properties within a particular simulation (Sections 4.2a, b, e). Percentiles with low or high values of p are useful for summarizing the tails of probability distributions and can easily be compared (Sections 4.1, 4.2c, 4.3a, c). Changes in percentiles can be related to changes in the location (e.g. mean) and scale (e.g. variance) of the distribution (Mearns *et al.*, 1984; Katz and Brown, 1992; Ferro *et al.*, 2005). Annual indices can also be summarized by sample statistics (Sections 4.1, 4.2e) and by fitting probability models (Section 4.2e).

[Table 1 near here please]

The severity of the events considered in this paper, and other events with critical impacts, is the subject of ongoing research in PRUDENCE. Determining severity is a cross-disciplinary problem because an event's impact on a system depends on the system's state. The economic impact of an extreme event on corn production, for example, depends not only on temperature and precipitation, but also on irrigation, market prices, land prices, production costs, agricultural policies such as subsidies, mitigation strategies, and available compensation. See Halsnaes (2004) for a detailed discussion of these issues. Once the roles of these different factors are understood, adaptations can be planned to counteract climate change predicted by models. Both the individual effects and the interactions of different factors can be crucial, with climatic thresholds or non-linear combinations potentially triggering severe impacts. Temporal and spatial patterns of events are also important. Table 2 lists some of the impacts related to the European climatic extremes discussed in this paper. Careful analysis is required to model the complex relationships between climate and these impacts on health, agriculture, forestry, infrastructure, and ecosystems.

[Table 2 near here please]

There is a clear incentive for the research community and the public and private sectors alike to focus on the future course of extreme climatic events under the changing climatic conditions expected during the 21st century. A better understanding of the factors involved will improve the quantification of costs associated with climate-related hazards and thereby provide the basis for strategies to adapt to climate change.

3. Data sets used: the RCM simulations

This section gives a brief overview of the PRUDENCE model data used in this paper. More details of the design of the model experiments are given in Jacob et al. (2005).

PRUDENCE has created a total of fifty-five, 30-year integrations employing nine regional climate models (RCMs) and one stretched global atmospheric model. Daily grid-point values of a range of climatic variables for each RCM integration have been made available on a purpose-built website database (<http://prudence.dmi.dk>). The PRUDENCE experiments include control simulations of contemporary (1961-90) climate and scenario simulations of future (2071-2100) climate. Lateral boundary conditions for the RCMs are supplied by one of two high-resolution, global atmospheric general circulation models (GCMs). Observed fields of sea-surface temperature (SST) and sea-ice extent (SICE) provide boundary conditions for the GCMs in the control period. Boundary conditions for the GCMs in the scenario period are constructed by adding to the observed fields anomalies (the differences between 2071-2100 and 1961-90) from integrations of the coupled atmosphere-ocean global model HadCM3 (Jones *et al.*, 2001; Johns *et al.*, 2003) forced with two greenhouse-gas emissions scenarios based on the A2 (high emissions) and B2 (lower emissions) ‘families’ of scenarios developed by the IPCC (Nakicenovic *et al.*, 2000).

The two GCMs designated to provide boundary conditions for the PRUDENCE RCM experiments are the UK Hadley Centre HadAM3H model (Pope *et al.*, 2000) at $1.875^\circ \times 1.25^\circ$ resolution in longitude and latitude, and the German Max-Planck-Institute ECHAM5 model (Roeckner *et al.*, 2003). Only experiments with HadAM3H boundaries have been performed in time for inclusion in this work. On the other hand, earlier RCM experiments driven directly with both lateral boundaries and SST/SICE from the ECHAM4/OPYC3 coupled ocean-atmosphere model (Roeckner *et al.*, 1996) are included in order to sample the dependence of results on the driving model. The HadAM3H model has been used to generate an ensemble of three control runs, all with observed SST/SICE, and an ensemble of three A2 scenario runs with SST/SICE anomalies from three different HadCM3 integrations. The HadAM3H and ECHAM4/OPYC3 global mean temperature responses were similar to one another for both the A2 scenario (3.1°C and 3.4°C respectively) and the B2 scenario (2.3°C and 2.6°C respectively), and are in the middle of the range of climate sensitivities (1.4°C to 5.8°C) given by IPCC (2001).

The output from all RCMs has been investigated but results are presented here for only the following models due to space limitations.

- HIRHAM model of the Danish Meteorological Institute (Christensen *et al.*, 1998),
- HadRM3H/P model of the Hadley Centre (Johns *et al.*, 2003),
- RCAO model of the Swedish Meteorological and Hydrological Institute (Räisänen *et al.*, 2004),
- REMO model of the Max-Planck-Institute of Meteorology (Jacob, 2001),
- CHRM model of the Swiss Federal Institute of Technology (ETH) (Lüthi *et al.*, 1996; Vidale *et al.*, 2004).
- CLM model of the Institute for Coastal Research (GKSS; Steppler *et al.*, 2003).
- RACMO2 model of the Royal Netherlands Meteorological Institute (KNMI; Lenderink *et al.*, 2003).
- Suffixes -E and -H will denote RCMs driven by the HadAM3H and ECHAM4/OPYC3 GCMs respectively; additional suffixes /C, /A2 and /B2 will denote GCMs forced by control, A2 and B2 scenario emissions.

4. Results

4.1 Heat waves

The heat wave that scorched much of Europe in the first two weeks of August 2003 (Beniston, 2004; Schär *et al.*, 2004) led to thousands of excess deaths in France, Italy and Spain (Fischer *et al.*, 2004; Stedman, 2004). This highlighted problems that could afflict environmental systems such as hydrology and ecosystems, socio-economic systems such as agriculture and energy supply, and human mortality and morbidity if such events were to increase in frequency, intensity, and persistence.

The incidence of summer heat waves increased during the course of the 20th century (IPCC, 2001; Frich *et al.*, 2002 at the global scale; Schär *et al.*, 2004 for Europe) and modeling studies (e.g. Zwiers and Kharin, 1998; Huth *et al.*, 2000; Kharin and Zwiers, 2000; Meehl *et al.*, 2000), most of which were based on GCM simulations, concluded that this trend is likely to continue through the 21st century. However, IPCC (2001) exercised caution over these conclusions, pointing to the lack of adequate data and analyses, and the need to improve both the accuracy and regional detail of model projections. Moreover, the wider literature mentions little about anomalously warm episodes outside the summer season. For instance, relatively mild periods during winter can adversely affect the environment and the economy by causing floods and poor skiing conditions, and by disrupting crop production (Beniston and Jungo, 2002; Beniston, 2003; Shabbar and Bonsal, 2003). This section investigates the changes in frequency, intensity and duration of summer heat waves and other unseasonably warm spells between the PRUDENCE control and A2 scenario simulations. Results for only HIRHAM-H are reported here; CHRM-H and RCAO-H were also analyzed and yielded similar results.

Several measures of extreme temperatures are used: the frequency with which daily maximum temperature exceeds 30°C, high temperature percentiles, and four heat-wave indices. A heat-wave is defined to be a spell of at least six consecutive days with maximum temperature exceeding the 1961-90 calendar day 90th percentile, calculated for each day over a centred 5-day window at each grid point (WMO, 1999; Robinson, 2001; Peterson *et al.*, 2001). The four indices, calculated for each year, are

- Heat Wave Number (HWN) – the number of heat waves,
- Heat Wave Frequency (HWF) – the total length (days) of all heat waves,
- Heat Wave Duration (HWD) – the maximum length (days) of all heat waves,
- Heat Wave Intensity (HWI) – the maximum threshold excess (degree days) of all heat waves.

The ability of HIRHAM-H to simulate temperature over Europe was evaluated by comparing maps of daily maximum temperature quartiles (not shown) to those from the NCAR/NCEP re-analysis data (<http://www.cdc.noaa.gov/cdc/reanalysis/>). HIRHAM-H/C reproduced the annual and seasonal patterns of these quartiles for the control period. Heat-wave indices from HIRHAM-H/C were also compared to those from thirteen station observation series (Klein Tank *et al.*, 2002) selected to give reasonable European coverage and records without artificial breaks between 1961 and 1990. HIRHAM-H/C reproduced the mean spatial patterns of 30°C exceedance frequency, and the four heat-wave indices agreed closely with most of the thirteen stations.

Figure 2 shows the mean number of days per year above 30°C simulated by HIRHAM-H/C and HIRHAM-H/A2. The summer climatic zones shift northward by at least 400-500 km by the end of the 21st century. Regions such as France and Hungary, for example, may experience as many days per year above 30°C in the future as are currently experienced in Spain and Sicily. The mean number of days per year exceeding 30°C at the model grid point nearest to Paris increases from nine days under current climate (observations at the Paris-Montsouris station give six days) to fifty days under future climatic conditions; whereas heat waves in Paris are restricted to summer (JJA) during the control period, 10% of the heat wave days occur outside summer in the scenario simulation; the maximum number of consecutive days per year exceeding 30°C at Paris increases from an average of 3.5 days (3.0 for observations at Paris-Montsouris) to 18.9 days.

High percentiles of daily maximum temperature across Europe generally increase more than lower percentiles, implying that changes in the PDFs are more than shifts in location. Following Ferro *et al.* (2005), the remaining percentage change in the 99th percentile was mapped after adjusting for changes in the median (Figure 3a) and in the median and interquartile range (Figure 3b). There is a substantial change in the 99th percentile (up to 60% in north-eastern Europe) not explained by change in the median alone. Shifts in scale help to explain most of the remaining changes in the 99th percentile. In other words, changes in the variance (as well as the mean) of daily maximum temperatures have a substantial impact on future extreme daily temperatures. Largest changes in variance were found over the continental interior (a latitude band encompassing France and Hungary; see also Schär *et al.*, 2004) and are most likely caused by a drying out of the land surface in warmer and drier future summer conditions.

Figure 4 shows the changes (expressed as ratios) in the four heat wave indices simulated by HIRHAM-H. The mean duration (HWD, Fig. 4a) increases by a factor of between one and eight over most of Europe. Much higher increases of at least a factor of seven are predicted for the mean intensity (HWI, Fig. 4b), the mean number of heat waves (HWN, Fig. 4c) and the frequency of heat-wave days

(HWF, Fig. 4d), with greatest changes (more than ten-fold increases) in the south of France and Spain. Further analyses, including seasonal comparisons, of simulations from three other GCM/RCM combinations in PRUDENCE confirm the above conclusions (Koffi, 2004).

4.2 Extreme precipitation

This section presents results for several diagnostics of heavy precipitation in RCM output and discusses the simulated change in heavy precipitation between contemporary and future climates.

4.2a Validation of RCM simulation of extreme precipitation

This sub-section investigates the ability of RCMs to reproduce extreme precipitation events under current climatic conditions by means of a case study for southern Germany, where a dense long-term network of observation stations is available from the German Weather Service. Simulated data from REMO-H/C (Jacob, 2001) are compared to the observations interpolated to the model grid. The generalized extreme-value (GEV) distribution is fitted to summer maximum 1-day and winter maximum 5-day precipitation totals at each grid point, pooling maxima from the eight neighboring points to increase precision. These 1-day and 5-day aggregations account for the different character and impact of extreme precipitation in the two seasons – European winter flooding is generally due to persistent large-scale precipitation whereas summer flooding is more often due to rapid localized convective activity. The 5-year return levels for both the observations and the simulations are calculated from the GEV fits.

Figure 5 compares the estimated return levels for the two southernmost federal states of Germany (Baden-Wuerttemberg and Bavaria). The 5-year return levels of daily precipitation in summer (Figs. 5a, b) are adequately represented in the model with lower values in the relatively flat north and higher values in the alpine region to the south. However, the spatial variability is underestimated in REMO-H/C, thereby leading to a slight overestimation in the north and underestimation in the south. This may be related to underestimated topographic differences in mountainous regions, where a horizontal resolution of 55 km is insufficient to resolve strong altitudinal gradients. The 5-year return levels of 5-day winter precipitation (Figs. 5c, d) are generally higher in the mountainous south than in the north, both in the observations and in REMO-H/C. The observations exhibit return levels above 80 mm in the east of Bavaria, whereas REMO-H/C has lower values of around 60 mm in the same region. Despite some shortcomings, it seems possible to simulate the spatial distribution and approximate magnitude of extreme precipitation events. This is also true for more extreme events such as 10- and

20-year return levels (Semmler and Jacob, 2004). Previous model evaluations confirm these findings for a range of RCMs in PRUDENCE and for standard indices of precipitation extremes (Frei *et al.*, 2003).

4.2b Extreme value modelling of changes in extreme precipitation

The simulated changes in precipitation extremes are presented in this sub-section. Four RCMs are selected for analysis: CHRM-H, HadRM3P-H, HadRM3H-H, and HIRHAM-H. Three ensemble members are available for each model in each period (1961-90 and 2071-2100) except for CHRM-H, which has only one member.

The GEV distribution is again fitted by maximum likelihood to summer maximum 1-day and winter maximum 5-day mean precipitation, this time independently at each grid point and separately for both the control and A2 scenario integrations from each RCM. Return levels are estimated for only those grid points with more than fifteen non-zero seasonal precipitation maxima, so excluding certain grid points in southern Europe. The statistical significances of changes are assessed by parametric resampling similar to Kharin and Zwiers (2000). Figure 6 displays the changes in 5-year return levels between the HIRHAM-H/C and HIRHAM-H/A2 time-slices in winter (Fig. 6a) and summer (Fig. 6b). The 5-year level is chosen, as opposed to more rare events, to avoid excessive noise in the climate-change signals (see also Frei and Schär, 2001; Frei 2003).

In winter there is an increase in the return level north of about 45°N and a decrease to the south, which is similar to the pattern of change for mean precipitation (e.g. Jones *et al.*, 2001; Räisänen *et al.*, 2004) at least on large scales. Over much of north-western Europe, Scandinavia and eastern Europe, the 5-year return level estimated from the scenario is at least as large as the 15-year return level of the control experiment, which implies a more than three-fold increase in frequency. In winter, results from the other models are very similar both in spatial distribution and magnitude. This is also evident from Fig. 6c, which shows for all RCMs the domain mean response of a number of precipitation statistics, including the return levels of extremes. The similarity of results implies that in winter the simulated change of precipitation extremes is relatively insensitive to the different physical parameterization schemes used in these RCMs. The differences for CHRM-H are primarily due to the fact that only a single ensemble member was used.

In summer, the extreme value analysis diagnoses a statistically significant decrease (at the 5% level) in the 5-year return level for HIRHAM-H over many southern parts of the continent and an increase over Scandinavia and north-eastern Europe (Fig. 6b). An interesting regional variation is found over parts

of central and eastern Europe where the return level increases despite the pronounced decrease in mean precipitation in these regions reported by Christensen and Christensen (2003). Although the large-scale pattern of change is similar for all models in summer, the quantitative change in the precipitation distribution varies considerably (Fig. 6d). Over central Europe, there is a prominent decrease of precipitation frequency in HadRM3H-H and HadRM3P-H, while precipitation intensity and heavy precipitation percentiles show little change. In contrast, for CHRM-H and HIRHAM-H the decrease in frequency is partly compensated for by an increase in precipitation intensity and the frequency of heavy events as shown by the return levels. Similar model sensitivities were found for the Mediterranean area. In contrast to winter precipitation extremes, these results imply that the magnitude of the change in summer heavy precipitation events critically depends on the RCM formulation.

4.2c Sensitivity of results to GCM boundary conditions

The large-scale circulation changes of RCM simulations generally depend on the differences between the boundary conditions of the driving GCMs. For example, the boundary conditions from the Hadley Centre HadAM3H experiment projects a more south-westerly flow in the North Sea in future winters, leading to a reduction of precipitation in central and northern Norway, while the boundary conditions from the Max-Planck-Institute's ECHAM4/OPYC3 model predict increased zonal flow in future winters leading to a large increase in precipitation over the whole of Norway. A set of four climate-change experiments has been applied to this part of the investigations, namely two different RCMs (HIRHAM and RCAO) each driven with two different sets of boundary conditions (HadAM3H and ECHAM4/OPYC3).

Figure 7 illustrates the RCM projections of changes in the 95th percentile of daily summer precipitation exceeding 1 mm between the control and A2 scenario. Only areas of statistically significant change (at the 5% level) are presented for each experiment. The amplitude of change in this quantity varies with both the GCM and the RCM. The left column, for simulations driven by ECHAM4/OPYC3, shows general increases over the North Atlantic, a region where there is little change for the HadAM3H-driven simulations in the right column. Considering the effect of the RCM, slightly larger increases are seen with RCAO than with HIRHAM over central Europe, and vice versa over eastern Europe. However, the patterns of change are coherent across Europe, with general increases north of the Alps and small areas with decreases in the south. Comparing this with the corresponding change in median precipitation, which is negative for all models, it can be concluded that the reduction in summer precipitation is caused by a reduction in the number of rainy days. Results for winter (not shown) show larger increases in the 95th percentile than in the median, but regionally varying results for the number of rainy days.

4.2d Sensitivity of results to future emission scenarios

We have seen above that large-scale patterns of projected changes in heavy precipitation are robust to RCM but not to GCM, but that magnitudes of changes vary with RCM, particularly in summer. An additional source of uncertainty is the future emission of greenhouse-gases and aerosols. This subsection discusses the sensitivity of the projected changes to emissions by analyzing responses to two different scenarios (A2 and B2).

The 30-year means of the winter and summer maximum 1-day and 5-day precipitation totals (designated as R1d and R5d respectively) for the periods 1961-90 and 2071-2100 were derived from the daily output of seven RCMs: HIRHAM, RCAO, HadRM3P/H, CHRM, REMO, RACMO2 and CLM. Four pairs of experiments include both the A2 and B2 runs, two of which were driven by the HadAM3H boundary forcing and two by the ECHAM4/OPYC3 forcing. After interpolating onto a common $0.5^\circ \times 0.5^\circ$ grid, the seasonal means were averaged over 20 sub-domains of Europe. Then the differences between the present-day and future averages were computed to represent the RCM-simulated changes in the two indices of heavy precipitation. Variation among ensemble members (available for HIRHAM-H/A2 and HadRM3P-H/A2) provides a rough guide to simulated natural variability.

The mean winter maximum 5-day precipitation total increases in every model bar one for the Central Europe domain (Fig. 8a). The projected increases are slightly lower than the simulated changes in mean winter precipitation and the mean winter 1-day maximum (not shown). The changes in R5d predicted under the B2 scenario are smaller than those predicted under the A2 scenario in two cases, and similar in the two other cases. The range of simulated increases for an equal lateral GCM forcing (HadAM3H) and emissions scenario (A2) is about 10%, reflecting the uncertainty arising from differences in model formulation and the internal variability of climate. The variation due to divergent GCM forcing is at least as large.

Elsewhere in Europe, the simulated responses in wintertime R5d generally resemble those found for Central Europe. Over the Mediterranean land areas, however, R5d decreases as well as mean precipitation in some model experiments. Over northern Europe, the simulated increases in winter mean R5d are generally smaller for the B2 than for the A2 scenario. In many other regions the uncertainty in changes in R5d due to natural variability is at least as large as the variation between emission scenarios.

While the summertime mean precipitation over Central Europe decreases in all RCM experiments, the mean summer maximum 1-day precipitation total is generally projected to either increase or remain virtually unaltered (Fig. 8b). However, simulations with a very large reduction in the summer mean precipitation show decreases in R1d as well, yet the decreases in R1d are smaller than those in the mean precipitation. A comparison between the A2 and B2 scenarios indicates that smaller emissions yield weaker changes over Central Europe. The differences due to the emissions scenario appear to be at least of the same magnitude as those due to natural variability. The largest uncertainty, however, arises from differences in model formulation.

In sub-domains over southern Europe, the projected changes in summer mean R1d range from -60% to +10% (not shown). In most cases the reduction is smaller for the B2 than for the A2 scenario. In northern Europe, on the other hand, there are no clear systematic differences between projected increases for the two emissions scenarios (not shown). The projected changes in R1d are almost invariably positive, up to about 40%, and are strongly model-dependent. For the summer mean precipitation in northern Europe, there is a qualitative inter-model disagreement, some experiments showing a decrease and others either an increase or negligible change.

Over most sub-domains, the projected percentage changes in the two indices of heavy precipitation are closely correlated with changes in mean precipitation, even more so in summer than in winter. As a rule of thumb, the projected percentage changes in the summer mean R1d may be approximated by adding a factor of about 20-35% to the corresponding changes in mean precipitation. The factor for the summer mean R5d (not shown) is smaller but nonetheless positive, revealing the fact that the intensity of individual precipitation events increases more (in northern Europe) or decreases less (in southern Europe) than the total number of wet days. In winter, the tendency to smaller increases in R5d than in mean precipitation might be explained by comparable increases in the number of wet days and the average precipitation intensity (see Fig. 6c).

The ranges in the projected changes in the two indices of heavy precipitation illustrate the uncertainties due to differences in the RCM formulation, the emissions scenarios and the GCM boundary conditions. However, these factors do not represent the full range of uncertainty discussed by the IPCC (2001). In that report, a wider range of radiative forcing and a larger set of GCMs (but not RCMs) were considered than in PRUDENCE. Assuming, as hinted by Fig. 8, that changes in heavy precipitation are associated with changes in mean precipitation, it is pertinent to examine how the latter is projected to alter on the basis of a larger set of GCMs. In addition to HadAM3H and ECHAM4/OPYC3, the set considered by the IPCC included the CCSP/NIES, CGCM2, CSIRO Mk2, GFDL R30 and NCAR DOE PCM models (IPCC 2001; see also Ruosteenoja *et al.*, this issue). It appears that about half of the experiments applying the A2 forcing and almost all simulations applying

the B2 forcing produced smaller decreases in the summer mean precipitation over Central Europe than the RCM simulations considered here. This suggests that the range of uncertainty in the change of summertime heavy precipitation is not fully captured by analyzing the present RCM output. For the winter mean precipitation total, there were no major differences between the PRUDENCE RCM and IPCC GCM projected changes.

4.2e Risk of Mediterranean drought

This sub-section summarizes the changes in Mediterranean drought conditions predicted by three RCMs: HadRM3P, HIRHAM, and RCAO forced with both HadAM3H and ECHAM4/OPYC3. Drought-related precipitation indices indicate considerable drying over much of the Mediterranean under the A2 scenario. The main features are reduced intensity precipitation, earlier onset and longer duration of drought. The regions most affected are the southern Iberian peninsula, the Alps, the eastern Adriatic seaboard, and southern Greece. Although the impacts are considerably reduced in the B2 scenario, which produces increased precipitation in some areas, the overall pattern is still one of a drier Mediterranean.

The changes simulated by the different RCMs are sufficiently similar that multi-model averages, with reduced variability, are meaningful. Figure 9 maps the average change for one index: the annual maximum length of dry spell (summer drought). The difference between the index, averaged over time and models, in the control period and in each of the A2 and B2 scenarios is calculated and uncertainty is represented by the width of bootstrapped 95% confidence intervals. Under the A2 scenario (Fig. 9a), drought over southern Iberia lasts over a month longer than at present, with a 95% confidence interval of about ± 9 days (Fig. 9b). Under the B2 scenario (Fig. 9c), the length of drought over southern Iberia increases by about 20 days with roughly the same uncertainty (Fig. 9d) as for the A2 scenario.

Changes in return levels of annual maximum length of wet spell are estimated by fitting the GEV distribution to annual maxima from the control and scenario simulations. Figure 10 maps the changes in 100-year return level and reveals a general reduction of about 15 to 20 days (or 40%) under the A2 scenario but by only 5 to 10 days (or 20%) under the B2 scenario. Changing the driving GCM, as seen in Figures 10c and 10e for RCAO-H and RCAO-E respectively, is more influential than changing the emissions scenario. This finding is consistent across all analyses of precipitation extremes and merits further investigation using different forcing models on other RCMs in future studies.

4.3 Extreme wind storms and storm surges

4.3a Wind storms

North Atlantic extra-tropical cyclones can often lead to high surface wind speeds in Europe, especially over the sea or in coastal and mountainous regions. Rapidly developing cyclones can produce anomalously severe weather, high winds and storm surges that devastate the natural environment and many socio-economic sectors (IPCC, 2001). It is therefore important to assess future storminess by investigating extremes in variables such as daily mean sea-level pressure, p_{msl} , 10-metre daily maximum wind speed, $v_{10,\text{max}}$, and 10-metre wind direction, $v_{10,\text{dir}}$. The mean and the tails of the PDFs of p_{msl} , $v_{10,\text{max}}$, and $v_{10,\text{dir}}$ fields are investigated here in control and for the IPCC A2 Scenario simulations from the HIRHAM-H, CHRM-H and RCAO-H models. We have focused on winter (DJF) when such storm activity is most vigorous, although storminess in other seasons can also lead to large impacts (e.g. the October 1987 storm that caused much damage in the south of England).

Prior to analyzing these changes, the simulated winter mean sea-level pressure and the 10-metre wind velocity fields were compared to the NCAR/NCEP reanalysis mean sea-level pressure and 1000-hPa wind speed and direction respectively. This comparison confirmed that the RCMs realistically reproduced the large-scale features of these quantities during the 1961-90 period. The mean sea-level pressure has a strong north-south gradient, from roughly 995 hPa south of Iceland to more than 1015 hPa in central Europe. Between these low- and high-pressure systems, the isobars are almost parallel and are tilted in a SW-NE direction. The mean DJF wind velocity vector field has a marked but smooth east-west gradient with stronger winds over the ocean. The mean wind speed ranges from 4 m/s inland to over 13 m/s over the central North Atlantic Ocean. The simulated 90th percentiles of wind speed exceed 20 m/s over the ocean, and are between 4 and 6 m/s over land but with a sharper east-west gradient component at the ocean-land transition region.

Zwiers and Kharin (1998) found evidence for increased extreme wind speeds related to a negative pressure anomaly over northern Europe in a doubled CO₂ integration of a Canadian GCM. RCM results give similar large-scale conclusions but also reveal more detail. The 90th percentile of daily DJF wind speeds show a 3-25% increase in a European latitude band extending roughly from 45-55°N, and the changes generally decrease to small or even negative values on either side of this band as shown in Figure 11 for RCAO-H. The positive changes are concentrated over the ocean, the North Sea, and western Europe (UK, France, northern Switzerland, Germany). The number of days exceeding the control period 90th percentile increases by up to 50% within the core, but outside the

Alps, during the 2071-2100 period as shown in Figure 12 for HIRHAM-H. Generally, over the continent, there is no obvious relationship between these changes and orography apart from the Alps where there seems to be a systematic positive change to the north and a negative change over and south of the Alps. Over Croatia, similar but less intense changes occur with the Dinaric Alps and the Dalmatian Coast to the west. Similar conclusions hold for changes in the mean value of wind velocity in each RCM. The 10th percentile of daily DJF sea-level pressure generally shows a 2-3 hPa decrease over the UK, the North Sea, the Norwegian Sea, the Baltic, extending inland to France, Germany, and Scandinavia. Negative anomalies of up to 5 hPa are seen in the mean DJF sea-level pressure (Figure 13) as well as in the 90th percentile fields under the A2 scenario. This corresponds to the negative pressure anomaly diagnosed in the Canadian GCM experiments, which intensifies the zonal circulation over Europe and brings more storms into this area following the North Atlantic storm tracks.

The Alpine mountain chain appears to be a locus of important changes in the behavior of the wind speeds and directions between current and future climates. The 10-metre wind speeds of the twenty-one HIRHAM-H model grid-points covering Switzerland have been analyzed in more detail for the two 30-year time-slices. The numbers of wind speed events per year exceeding the control period 95th and 99th percentiles and falling below the 25th percentile all increase by 10% (not shown). The most substantial increases occur in winter, when there is a three-fold increase in the number of events exceeding the 99th percentile north of the Alps, but also a notable reduction over and south of the Alps. In summer there is a marked increase in the number of events below low thresholds, indicating that calmer conditions are projected to occur in this season. An analysis of the simulated wind directions indicates that, during winter, the frequency of north-westerly winds will increase by up to 7% and south-westerly flows will decrease by a similar amount over Switzerland. These results agree with Stefanicki *et al.* (1998) and Schiesser *et al.* (1997). Such conditions could lead to an enhanced occurrence of extreme windstorms such as the February 1990 *Vivian* storm or the December 1999 *Lothar* storm.

In summary, this preliminary analysis has found an increase in high percentiles of the wind velocity fields of up to 25% in a 10° latitude band centered at 50°N over the ocean and over western Europe, especially north of the Alps and stretching to the Baltic Sea. Although not very extreme in terms of velocities, intense wind episodes are likely to be more frequent on average according to many RCM simulations for 2071-2100.

4.3b Modeling of storm surges

Over the last century, floods have severely impacted coastlines of the North Sea. These floods have damaging impacts that threaten human life as well as property. For a given stretch of coastline, the extent of a storm flood depends directly on wind speed and wind direction. When winds push water towards the coast, it tends to accumulate in a *storm surge*. Serious flooding usually results when a high surge occurs together with a tidal maximum. Flather *et al.* (1998) and Kauker and Langenberg (2000) among others have shown that the long-term statistics of storm surges can be modeled satisfactorily with hydrodynamic models. Barotropic models, which operate with vertically integrated state variables, are sufficient for modeling water level variations around the North Sea (Kauker and Langenberg, 2000).

Such models can be used not only to reconstruct the past history of water-level variations and storm surges along the North Sea coast (Langenberg *et al.*, 1999), but also to estimate possible future storm surge statistics (Flather and Smith, 1998; Langenberg *et al.*, 1999; Lowe *et al.*, 2001; Kaas *et al.*, 2001). Scenarios are obtained by running the hydrodynamic model twice: first with wind and pressure conditions simulated by a high-resolution RCM under ‘control’ conditions (i.e. with present day atmospheric greenhouse gas loadings) and then under enhanced greenhouse gas concentrations. In the WASA project (Langenberg *et al.*, 1999; Flather and Smith, 1998) the wind and pressure data were obtained from two 5-year simulations, in comparison to the 30-year time slices that were used in STOWASUS project (Kaas *et al.*, 2001). A barotropic hydrodynamic model has also been used in PRUDENCE to conduct paired control and climate-change simulations, but differs from previous studies by dynamically downscaling the regional wind and pressure conditions. This enables changes in storm surge statistics to be assessed using two of the RCM simulations: HIRHAM-H and RCAO-H.

The hydrodynamic model used here is the barotropic storm surge model TRIMGEO (Tidal Residual and Intertidal Mudflat model) developed by Casulli and Catani (1994). The model grid resolution is $6' \times 10'$ in latitude and longitude, which corresponds to a grid box size of about $10 \times 10 \text{ km}^2$. The integration time step is 10 minutes; the meteorological forcing is prescribed at the surface as a linear interpolation of 6-hourly instantaneous values. At the open boundaries, in the English Channel and along a line between Wick (UK) and Karmøy (Norway), the sea level is prescribed by amplitudes and phases of seventeen partial tides. Aspelien and Weisse (2005) described the skill of the TRIMGEO model in simulating North Sea water levels. They demonstrated the capability of the tide-surge model to provide reconstructions of sea level heights and surge for the southern North Sea shelf for the period 2000 to 2002. For this study, the TRIMGEO model was driven with atmospheric hind-cast simulations performed with the 50 km-grid regional model SN-REMO (SN = spectral nudging; REMO, see Jacob *et al.*, 1995), forced by NCEP/NCAR large-scale re-analyses (Feser *et al.*, 2001).

Results indicated that the TRIMGEO model is able to reproduce sea level heights and surge statistics satisfactorily even without data-assimilation of tide gauge data. Discrepancies arise if local observations are compared with contemporaneous model data because of the near-shore water-level offset of the former and a temporal phase shift of the latter.

Water-level variations from an additional tidal simulation, forced only by water-level variations at the open boundaries of the model caused by the global astronomical tidal dynamics, were subtracted from the water-level variations obtained in the control and climate-change experiments to infer wind- and pressure-related surge residuals. This helps to highlight the effects of changes in storm characteristics such as intensity and storm track due to only meteorological forcing. The effect of the expected rise in mean sea level due to the changing volume of the global ocean is not taken into account.

4.3c Changes in surge-related storminess

Important changes in storminess relevant to North Sea storm surges will be briefly discussed here.

Figure 14 shows changes in the 99th percentile of 10-metre wind speed for winds blowing from a westerly sector, the wind direction with highest impact on storm surge evolution. Wind velocity increases by up to 1.5 m/s over large areas of the North Sea in the RCAO model, and by up to 2 m/s in HIRHAM-H. The differences between RCMs have implications for the resulting storm surge statistics, as will be seen later.

[Table 3 near here please]

Table 3 summarizes changes in the frequency of severe storms. The number of storms is determined by the frequency with which wind thresholds of 17.2 m/s (Beaufort 8; “gale”), 20.8 m/s (Beaufort 9) or 24.5 m/s (Beaufort 10; “storm”) are exceeded (Weisse *et al.*, 2004) during winter (DJF). Results are presented for hindcasts of the 1961-90 period (Feser *et al.*, 2001) and for both the control and A2-scenario runs of HIRHAM-H and RCAO-H in nine selected grid boxes. The control simulations of both RCMs generate markedly fewer gale and storm events than the hindcast experiment. For gales, the ratio between the number of simulated and hindcast events varies between 33 and 85%, for storms between 60 and 70%. Very strong storms (>32.7 m/s or Beaufort 12) are formed, albeit rarely, in the hindcast, but never in the control or scenario simulations. The number of moderate storms (Beaufort 8) increases by up to 55% from the control to the A2 scenario in most of the nine grid boxes with RCAO-H, but by only up to 30% with HIRHAM-H. In contrast, the number of strong storms (Beaufort 9)

increases by up to 100% in HIRHAM-H but only 50% in RCAO-H. This divergence between the models continues at higher wind speeds.

In summary, both the intensity of westerly wind speed extremes and the number of North Sea gales increase in both RCM simulations and so increases in storm surges are likely. Detailed analysis of future changes in near surface wind speed extremes over Europe and differences due to RCM formulations can be found in Rockel and Woth (2006).

4.3d Changes in North Sea coastal storm surges

The impact of the changes in meteorological conditions for the storm surge statistics is evaluated through the changes in percentiles of the TRIMGEO simulated high water elevation. Since most damage is expected in the coastal zone (Langenberg *et al.*, 1999), storm surge residuals were analyzed for 209 grid cells along the North Sea coast. Figure 15 shows the TRIMGEO integration area, the bathymetry as well as the 209 coastal grid points located along the North Sea coast, extending from Wick (UK) to Skagen (Denmark).

Figure 16 compares the modeled surge forced with RCAO-H and HIRHAM-H data for present-day conditions and for the A2 scenario. The maximum of the modeled surge for each year was selected and averaged across each of the two 30-year periods. The grey shaded band marks 90% confidence intervals based on Student's t distribution and inter-annual natural variability in the control run (von Storch and Zwiers, 1999). Scenario averages falling outside this band indicate significant changes. Along the UK coast, the A2 scenario curve remains within the grey band, indicating no significant change in surge statistics. Along the Dutch, German and Danish coasts, however, the curve is above the grey band, suggesting an increase in the mean maximum winter surge for the A2 scenario. The increase reaches almost 60 cm for the HIRHAM-H forcing but only 25 cm for RCAO-H. This difference between the HIRHAM-H and RCAO-H simulations is fully consistent with the analyzed change in maximum wind values alluded to earlier. More details are in Woth *et al.* (2004).

As expected, changes in winter storminess lead to increased sea-level surges along the North Sea coast, especially in Holland, Germany and Denmark, where the largest storm surges presently occur.

5. Conclusions

We focused on heat waves, heavy precipitation events, drought, winter storms, and resulting sea surges because of their large impacts on Europe. A variety of diagnostic methods were applied to determine how these events are predicted to change by the end of the 21st century in the set of PRUDENCE RCM experiments. A summary of the main results follows.

- Heat waves – Regional surface warming causes the frequency, intensity and duration of heat waves to increase over Europe. By the end of the 21st century, countries in central Europe will experience the same number of hot days as are currently experienced in southern Europe. The intensity of extreme temperatures increases more rapidly than the intensity of more moderate temperatures over the continental interior due to increases in temperature variability.
- Precipitation – Heavy winter precipitation increases in central and northern Europe and decreases in the south; heavy summer precipitation increases in north-eastern Europe and decrease in the south. These changes, which are weaker for the B2 than for the A2 scenario, are more robust to RCM in winter than in summer and reflect changes in mean precipitation. The RCMs all predict earlier and longer droughts in the Mediterranean.
- Winter storms – Extreme wind speeds increase between 45°N and 55°N, except over and south of the Alps, and become more north-westerly. These changes are associated with reductions in mean sea-level pressure and generate more North Sea storms, leading to increases in storm surge along the North Sea coast, especially in Holland, Germany and Denmark.

This paper has presented highlights from the most comprehensive regional climate change study performed for Europe. Many intriguing and pressing issues have emerged and many more studies now need to be performed to dig deeper into the initial findings presented here. Perhaps one of the major weaknesses of this project is that boundary conditions have been provided by only two GCMs so that the full spectrum of possible transient scenarios has not been fully sampled.

Despite the uncertainties present in these model simulations of future climate, it is clear that the regional changes in extremes presented here will cause Europe to face some major societal challenges in forthcoming decades.

6. Acknowledgements

The majority of this work has been funded by the European Union Framework 5 project PRUDENCE (EVK2-CT-2100-00132). The Swiss partners of PRUDENCE received funding from the Swiss Ministry for Education and Research. ETH also received funding from the EU project STARDEX (EVK2-CT-2001-00115). We wish to thank other participants of the PRUDENCE project for their invaluable comments on this work.

7. References

- Aspelien, T. and R. Weisse, 2005: Assimilation of Sea Level Heights into a Regional Ocean Model for the North Sea. Submitted to Ocean Dynamics.
- Beniston, M., 2003: Climatic change in mountain regions: a review of possible impacts. *Climatic Change*, 59, 5-31.
- Beniston, M., 2004: The 2003 heat wave in Europe: A shape of things to come? *Geophys. Res. Letters*, 31, L02202.
- Beniston, M., and P. Jungo, 2002: Shifts in the distributions of pressure, temperature and moisture in the alpine region in response to the behavior of the North Atlantic Oscillation. *Theoretical and Applied Climatology*, 71, 29-42.
- Casulli, V. and E. Cattani, 1994: Stability, Accuracy and Efficiency of a Semi-Implicit Method for Three-Dimensional Shallow Water Flow. *Computers Math Applic* 27: 99—112.
- CDC. Data provided by the NOAA-CIRES Climate Diagnostics Center, Boulder, Colorado, from their Web site at <http://www.cdc.noaa.gov/>.
- Christensen, O. B., J. H. Christensen, B. Machenhauer, and M. Botzet, 1998: Very High-Resolution Regional climate Simulations over Scandinavia –Present Climate, *J. Clim.*, 11, 3204-3229.
- Christensen, J.H. and O.B. Christensen, 2003: Severe summertime flooding in Europe. *Nature*, 421, 805-806.
- Coles, S., 2001: An introduction to statistical modeling of extreme values. Springer, London.
- Ferro, C.A.T., A. Hannachi and D.B. Stephenson, 2005: Simple non-parametric techniques for exploring changing probability distributions of weather. Submitted to *J. Climate*.
- Feser, F., R. Weisse and H. von Storch, 2001: Multidecadal atmospheric modelling for Europe yields multi-purpose data. *EOS* 82, 305+310.
- Fischer, P.H., B. Brunekreef and E. Lebret, 2004: Air pollution related deaths during the 2003 heat wave in the Netherlands, *Atmos. Env.*, 38, 1083-1085.
- Flather, R. and J. Smith, 1998: First estimates of changes in extreme storm surge elevations due to doubling CO₂. *Global Atmos Ocean Sys* 6: 193 – 208.
- Flather, R., J. Smith, J. Richards, C. Bell and D. Blackman, 1998: Direct estimates of extreme surge elevations from a 40 year numerical model simulation and from observation. *Global Atmos Ocean Sys* 6: 165 – 176.
- Frei, C., 2003: Statistical limitation for diagnosing changes in extremes from climate model simulations. Proc. 14th Sympos. on Global Change and Climate Variations. AMS Annual Meeting 2003, Long Beach, CA. On CD-ROM, 6 pp.
- Frei, C. and C. Schär, 2001: Detection probability of trends in rare events: Theory and application to heavy precipitation in the Alpine region. *J. Climate*, 14, 1564-1584.
- Frei, C., J.H. Christensen, M. Déqué, D. Jacob, R.G. Jones and P.L. Vidale, 2003: Daily precipitation statistics in regional climate models: Evaluation and intercomparison for the European Alps. *J. Geophys. Res.*, 108 (D3), 4124 doi:10.1029/2002JD002287.
- Frich, P., L.V. Alexander, P. Della-Marta, B. Gleason, M. Haylock, A.M.G. Klein Tank, and T. Peterson, 2002: Observed coherent changes in climatic extremes during the second half of the twentieth century, *Climate Research*, 19, 193-212.
- Halsnaes, K., 2004: Climate Change Impacts and Adaptation Analysis – How to Link Physical Climate Data and Economic Studies, Working Paper of the Prudence project. UNEP Risø Centre, Denmark.
- Huth, R., J. Kysely and I. Pokorna, 2000: A GCM simulation of heat waves, dry spells, and their relationships to circulation. *Clim Change* 46: 29-60.
- IPCC, 2001: Climate Change 2001: The Scientific Basis. Contribution of Working Group I to the Third Assessment Report of the Intergovernmental Panel on Climate Change. Houghton T., Ding Y., Griggs D.J., Noguer M., van der Linden P.J., Da X., Maskell K. & Johnson C.A. (eds.), Cambridge University Press, 881 pp.

- Jacob, D., 2001: A note to the simulation of the annual and interannual variability of the water budget over the Baltic Sea drainage basin. *Meteorology and Atmospheric Physics*, 77, 61-73.
- Jacob, D., R. Podzun and M. Claussen, 1995: REMO - A Model for Climate Research and Weather Prediction. International Workshop on Limited-Area and Variable Resolution Models, Beijing, China, October 23-27, 1995, 273-278.
- Jacob, D., et al., 2005: An intercomparison of regional climate models for Europe: design of the experiments and model performance. This issue, Chapter 1.
- Johns, T.C., et al., 2003: Anthropogenic climate change for 1860 to 2100 simulated with the HadCM3 model under updated emission scenarios, *Clim. Dyn.*, 20, 583-612.
- Jones, R., J. Murphy, D. Hassell and R. Taylor, 2001: Ensemble mean changes in a simulation of the European climate of 2071-2100, using the new Hadley Centre regional climate modelling system HadAM3H/HadRM3H. Hadley Centre Report 2001, available from prudence.dmi.dk.
- Kaas, E., U. Andersen, R.A. Flather, J.A. Willimas, D.L. Blackman, P. Lionello, F. Dalan, E. Elvini, A. Nizzero, P. Malguzzi, A. Pfizenmayer, H. von Storch, D. Dillingh, M. Phillipart, J. de Ronde, M. Reistad, K.H. Midtbø, O. Vignes, H. Haakenstad, B. Hackett, I. Fossum and L. Sidselrud, 2001: Synthesis of the STOWASUS-2100 project: Regional storm, wave and surge scenarios for the 2100 century. Danish Climate Centre Report 01-3, 22pp.
- Katz, R.W. and B.G. Brown, 1992: Extreme events in a changing climate: Variability is more important than averages, *Climate Change*, 21, 289-302.
- Kauker, F. and H. Langenberg, 2000: Two models for the climate change related development of sea levels in the North Sea. A comparison. *Clim. Res.* 15, 61-67.
- Kharin, V.V. and F.W. Zwiers, 2000: Changes in the extremes in an ensemble of transient climate simulations with a coupled Atmosphere-Ocean GCM. *J. Climate*, 13, 3760-3788.
- Klein Tank, A.M.G., J. B. Wijngaard, G. P. Können, R. Böhm, G. Demarée, A. Gocheva, M. Mileta, S. Pashiardis, L. Hejkrlik, C. Kern-Hansen, R. Heino, P. Bessemoulin, G. Müller-Westermeier, M. Tzanakou, S. Szalai, T. Pálsdóttir, D. Fitzgerald, S. Rubin, M. Capaldo, M. Maugeri, A. Leitass, A. Bukantis, R. Aberfeld, A. F. V. van Engelen, E. Forland, M. Mietus, F. Coelho, C. Mares, V. Razuvaev, E. Nieplova, T. Cegnar, J. Antonio López, B. Dahlström, A. Moberg, W. Kirchhofer, A. Ceylan, O. Pachaliuk, L. V. Alexander, P. Petrovic, 2002. Daily dataset of 20th-century surface air temperature and precipitation series for the European Climate Assessment, *Int. J. Climatol.*, 22, 1441-1453.
- Koffi, B., 2004: Heat waves in Europe by the end of the 21st century: Analysis of multi regional climate simulations. *Clim. Dyn.* submitted.
- Langenberg, H., A. Pfizenmayer, H. von Storch and J. Sündermann, 1999: Storm related sea level variations along the North Sea coast: natural variability and anthropogenic change.- Cont. Shelf Res. 19: 821-842.
- Lenderink, G., van den Hurk, B., van Meijgaard, E., van Ulden, A., and Cuipers, H., 2003: Simulations of present-day climate in RACMO2: first results and model development. Royal Netherlands Meteorological Institute Technical Report, De Bilt, The Netherlands.
- Lowe J.A., J.M. Gregory and R.A. Flather, 2001: Changes in the occurrence of storm surges around the United Kingdom under a future climate scenario using a dynamic storm surge model driven by the Hadley Centre climate models.
- Lüthi, D., A. Cress, H.C. Davies, C. Frei and C. Schär, 1996: Interannual variability and regional climate simulations. *Theor. Appl. Climatol.*, 53, 185-209.
- Mearns L.O., R.W. Katz and S.H. Schneider, Extreme high-temperature events, 1984: Changes in their probabilities with changes in mean temperature, *Journal of Climate and Applied Meteorology*, 23, 1601-1613.
- Meehl G.A., F. Zwiers, J. Evans, T. Knutson, L. Mearns, P. Whetton, 2000: Trends in extreme Weather and Climate Events: Issues related to modelling extremes in projections of future climate change. *Bull Am Meteorol Soc* 81: 427-436.
- Munich Re, 2002 : Topics, An annual review of natural catastrophes. Munich Reinsurance Company Publications, Munich, 49 pp.
- Nakićenović, N., J. Alcamo, G. Davis, B. de Vries, J. Fenner, S. Gaffin, K. Gregory, A. Grübler, T.Y. Jung, T. Kram, E.L. La Rovere, L. Michaelis, S. Mori, T. Morita, W. Pepper, H. Pitcher, L. Price, K. Raihi, A. Roehrl, H-H. Rogner, A. Sankovski, M. Schlesinger, P. Shukla, S. Smith, R.

- Swart, S. van Rooijen, N. Victor, Z. Dadi, 2000: IPCC Special Report on Emissions Scenarios, Cambridge University Press, Cambridge, United Kingdom and New York, NY, USA, 599 pp.
- Peterson, T.C., C. Folland, G. Gruza, W. Hogg, A. Mokssit and N. Plummer, 2001: Report on the Activities of the Working Group on Climate Change Detection and related Rapporteurs, 1998-2001, Report WCDMP-47, WMO-TD 1071.
- Pope, D.V., M. Gallani, R. Rowntree and R. A. Stratton, 2000: The impact of new physical parameterizations in the Hadley Centre climate model HadAM3, *Climate Dynamics*, 16, 123-146.
- Räisänen, J., Hansson, U., Ullerstig, A., Döscher, R., Graham, L.P., Jones, C., Meier, M., Samuelsson, P. and Willén, U., 2004: European climate in the late 21st century: regional simulations with two driving global models and two forcing scenarios. *Clim. Dynamics*, 22, 1, 13-31.
- Reich, T., 2001: Langzeitverhalten von Gebietsniederschlägen - Ergebnisse aus KLIWA. *KLIWA-Berichte*, Heft 1. Arbeitskreis KLIWA. Landesanstalt für Umweltschutz Baden-Württemberg, Bayerisches Landesamt für Wasserwirtschaft, Deutscher Wetterdienst (<http://www.kliwa.de/de/ergebnisse/content2vortrag3.html>).
- Robinson, P.J., 2001: On the definition of a Heat Wave. *J Appl Meteorol* 40: 762-775.
- Rockel, B. and K. Woth, 2006: Future changes in near surface wind speed extremes over Europe from an ensemble of RCM simulations. In preparation.
- Roeckner, E., K. Arpe, L. Bengtsson, M. Christoph, M. Claussen, L. Dümenil, M. Esch, M. Giorgetta, U. Schlese, and U. Schulzweida, 1996: The atmospheric general circulation model ECHAM4: Model description and simulation of present-day climate, *MPI Report* 218, Hamburg, Germany
- Roeckner E., et al., 2003: The atmospheric general circulation model ECHAM 5. PART I: Model description, *MPI-Report* 349, Hamburg, Germany
- Ruosteenoja, K., Tuomenvirta, H. and K. Jylhä, 2005: GCM-based regional temperature change estimates for Europe under four SRES scenarios. *This issue*
- Schär, C., P. L. Vidale, D. Lüthi, C. Frei, C. Häberli, M. Liniger and C. Appenzeller, 2004: The role of increasing temperature variability in European summer heatwaves, *Nature*, 427, 332-336.
- Schiesser H. H., C. Pfister, and J. Bader, 1997: Winter storms in Switzerland North of the Alps 1864/65–1993/94. *Theor. Appl. Climatol.*, 58, 1–19.
- Semmler, T., and D. Jacob, 2004: Modelling extreme events - a climate change simulation over Europe using the regional climate model REMO. *Planetary and Global Change*, submitted.
- Shabbar, A. and B., Bonsal, 2003: An assessment of changes in winter cold and warm spells over Canada, *Natural Hazards*, 29, 173-188.
- Stedman, J.R., 2004: The predicted number of air pollution related deaths in the UK during the August 2003 heatwave, *Atmos.Env.*, 38, 1087-1090.
- Stefanicki G., Talkner P., Weber R.O., 1998: Frequency changes of weather types in the Alpine region since 1945. *Theor. Appl. Climatol.*, 60, 47-61.
- Steppler, J., G. Doms, U. Schättler, H. W. Bitzer, A. Gassmann, U. Damrath, and G. Gregoric, 2003: Meso-gamma scale forecasts using the nonhydrostatic model LM, *Meteorol. Atm. Phys.*, **82**, 75-96
- Swiss Re, 2003: Natural catastrophes and reinsurance. Swiss Reinsurance Company Publications, Zürich, 47 pp.
- Vidale, P.L., D. Lüthi, C. Frei, S. Seneviratne, C. Schär, 2004: Predictability and uncertainty in a regional climate model, *J. Geophys. Res.*, in press.
- von Storch, H., and F.W. Zwiers, 1999: Statistical Analysis in Climate Research, Cambridge University Press, ISBN 0 521 45071 3, 494 pp.
- Weisse R., H. von Storch and F. Feser, 2004: Northeast Atlantic and North Sea storminess as simulated by a regional climate model 1958-2001 and comparison with observations. *Clim. Res.* (In press).
- Wijngaard, J.B., A.M.G. Klein Tank and G.P. Konnen, 2003: Homogeneity of 20th century European daily temperature and precipitation series. *Int. J. of Climatol.*, 23, 679-692.
- WMO, 1999: Meeting of the Joint CCI/CLIVAR Task Group on Climate Indices, Bracknell, UK, 2-4 September 1998, Folland, C.K.; Horton, E.B.; Scholefield, P.R. (Eds), World Climate Data and Monitoring Programme, WCDMP-No.37, WMO-TD No. 930.
- Woth K., R. Weisse, H. von Storch et al, 2004: Dynamical modelling of North Sea storm surge climate: An ensemble study of storm surge extremes expected under possible future climate

conditions as projected by four different Regional Climate Models. Submitted to Int. J. of Climatol.

Zwiers, F. W., and V. V. Kharin, 1998: Changes in the extremes of the climate simulated by CCC GCM2 under CO₂ doubling. J. Climate, 11, 2200-2222.

	Maxima	Percentiles	Indices
Temperature		99th percentile of daily maximum temperature	Number of exceedances of 30°C; number, frequency, duration, and intensity of heat waves (6 consecutive exceedances of 90th temperature percentile)
Precipitation	Return levels of maximum summer 1-day and winter 5-day totals; annual maximum dry- and wet-spell lengths	95th percentile of summer 1-day totals	Means of maximum summer 1-day and winter 5-day totals
Wind storms	Annual maximum storm surge	90th and 99th percentiles of winter 10-metre wind speed; 10th percentile of winter sea-level pressure	Number of exceedances of 90th, 95th and 99th wind-speed percentiles; number of exceedances of Beaufort thresholds

Table 1: The extreme events considered in Section 4.

	Health	Agriculture	Forestry	Buildings and infrastructure	Ecosystems
Heat waves	Excess illness and mortality	Animal stress, crop damage	Impaired growth, pests	Increased cooling energy demand	Wildlife stress
Precipitation	Floods, poor water quality and adequacy	Crop failure by drought or excess water	Water stress	Floods, landslides, ground shrinkage, property loss	Soil erosion, water stress
Wind storms	Accidents	Crop damage	Timber loss, insect damage	Building damage	Reduced biodiversity
Wind surges	Floods	Floods and erosion	Floods and erosion	Floods and erosion	Floods and erosion
Adverse combinations	Temperature and moisture	Temperature, precipitation, and wind	Temperature, precipitation, and wind	Wind and floods	Unseasonable temperature, precipitation

Table 2: Typical impacts associated with extreme events.

		HIRHAM	1	2	3	4	5	6	7	8	9
Bf. 8	CTL	196	201	124	140	128	109	90	83	75	
	HC – CTL	28	42	59	79	78	55	59	53	49	
	A2 – CTL	-5	11	8	22	19	31	22	32	19	
Bf. 9	CTL	25	31	15	16	11	11	11	8	8	
	HC – CTL	62	43	44	35	31	39	17	27	28	
	A2 – CTL	18	13	10	14	15	10	4	10	10	
Bf. 10	CTL	3	3	0	0	0	0	0	0	0	
	HC – CTL	16	8	7	10	8	8	4	7	4	
	A2 – CTL	3	7	4	3	1	2	4	1	1	

		RCAO	1	2	3	4	5	6	7	8	9
Bf. 8	CTL	202	195	141	161	127	122	90	121	67	
	HC – CTL	22	48	42	58	79	42	59	15	57	
	A2 – CTL	7	4	47	38	36	71	45	48	31	
Bf. 9	CTL	29	31	15	15	11	10	6	9	4	
	HC – CTL	58	43	44	36	31	40	22	26	32	
	A2 – CTL	15	17	6	6	9	8	5	9	6	
Bf. 10	CTL	2	4	0	0	0	0	0	0	0	
	HC – CTL	17	7	7	10	8	8	4	7	4	
	A2 – CTL	2	-1	2	1	1	1	2	0	1	

Table 3: Numbers of Beaufort (Bf.) 8, 9 and 10 storms in nine $50 \times 50 \text{ km}^2$ grid boxes (marked on Fig. 15) in 30-year control (CTL) runs of the HIRHAM-H and RCAO-H models, and differences with a hindcast (HC) and scenario (A2) runs.

Figure captions

Figure 1: Relative importance of natural hazards as compiled by the Munich Reinsurance Company (2002), for billion-dollar events since 1950. Ordinate indicates the percentage of the total of each category, figures next to each sub-element of the histograms refer to the absolute amounts in each category.

Figure 2: Mean annual number of days above 30°C simulated by the HIRHAM4 regional climate model for the 1961-1990 (upper) and 2071-2100 (lower) periods.

Figure 3: Change (%) in the 99th percentile of summer (JJA) daily maximum temperature between the 1961-1990 and 2071-2100 periods after adjusting for the change in the median (upper), and in the median and scale (lower), based on HIRHAM4 simulations.

Figure 4: Changes (expressed as a ratio) in the heat wave indices N_HW (a), HW_F (b), HW_D (c) and HW_I (d) between the 1961-1990 and 2071-2100 periods, based on HIRHAM4 simulations. (See text for details and definitions of these indices).

Figure 5: 5-year return level of daily precipitation in summer (JJA) in mm for the period 1961-1990 for Baden-Wuerttemberg and Bavaria using the REMO model (a) and from observations by the German Weather Service (b). Frames (c) and (d) are the same as (a) and (b) but for 5-daily precipitation in winter (DJF). The black lines indicate the federal states of Baden-Wuerttemberg (west) and Bavaria (east).

Figure 6: a) Distribution of 5-year return level of 5-day precipitation in winter as simulated by the HIRHAM regional climate model. b) Same as (a) but for the 1-day precipitation extreme in summer. The change is given in terms of the ratio of return levels between the scenario and control time slices and the statistical significance (p -value = 5%) of the change (as determined by parametric resampling) is displayed as a bold black line. c) Relative change of several statistics of daily precipitation in winter as simulated by 4 RCMs (see legend). FRE: Frequency of wet days (daily amount larger than 1mm), MEA: mean seasonal precipitation, INT: precipitation intensity (average amount on wet days), q90: 90% quantile of wet days, $nXjD$ n -year return value of j -day extreme. d) Same as (c) but for summer.

Figure 7: The relative change in the 95th percentile of daily precipitation exceeding 1 mm from 1961-1990 to 2071-2100 for summer (JJA). Upper row: The HIRHAM regional model. Lower row: The RCAO regional model. Left column: Boundaries from ECHAM4/OPYC. Right column: Boundaries from HadAM3H. Only areas where the change of the 95th percentile is significant at the 95% significance level are shown.

Figure 8: Projected area-averaged changes (%) in the 30-year means of the greatest (a) 5-day precipitation total in winter and (b) 1-day precipitation total in summer in Central Europe (land areas in 47.0–54.0°N, 5.0–20.5°E), relative to the baseline period 1961–1990. Both variables are given as a function of the seasonal mean precipitation changes. The legend indicates the regional climate models, GCM forcing (HC referring to HadAM3H, HCP to HadAM3P, EC to ECHAM4/OPYC), the SRES emissions scenario (A2 or B2), and the number (in parentheses) of ensemble simulations.

Figure 9: a) A2a: Maximum dry spells (days); b) A2a confidence range (days); c) B2a: Maximum dry spells (days); d) B2a confidence range (days)

Figure 10: 100-year return levels of maximum length of wet spells for the following models: a) HadRM3P A2a; b) HadRM3P B2a; c) SMHI-HC A2a; d) SMHI-HC B2a; e) SMHI-MPI A2a; f) SMHI-MPI B2a; g) DMI A2a

Figure 11: Simulation by the RCAO regional climate model of the change (%) in the 90th percentile of winter (DJF) daily maximum wind speed in Europe, between the 1961-1990 and the 2071-2100 periods. Positive change is drawn in dotted line

Figure 12: Simulation by the HIRHAM4 regional climate model of the change (%) in the number of days in winter (DJF) where maximum wind velocity at 10 m exceeds the 90% quantile (based on the 1961-1990 baseline), between the 1961-1990 and the 2071-2100 periods.

Figure 13: Simulation by the CHRM regional climate model of the change (hPa) in the winter (DJF) mean of the Mean Sea Level Pressure in Europe, between the 1961-1990 and the 2071-2100 periods. Positive change is drawn in dotted line.

Figure 14: Changes between control and A2 simulations for the HIRHAM (left) and RCAO (right) models in the mean of 30 intra-annual 99% quantiles in 10m wind speed conditioned for a westerly direction.

Figure 15: TRIM integration area, the bathymetry (isolines) and the 209 near-coastal grid cells (crosses) located along the North Sea coast. The numbered locations indicate the selected grid cells for the ‘storm count’ (see Table 3)

Figure 16: Mean of winter maximum surge levels in meters from the 30-year control simulation (black line) and A2 SRES scenario (grey line) for 209 near-coastal locations along the North Sea coast (indicated as crosses in Fig. 4.3.4). Left: HIRHAM model, right: RCAO model. Shaded area: 90% confidence interval for present natural variability.

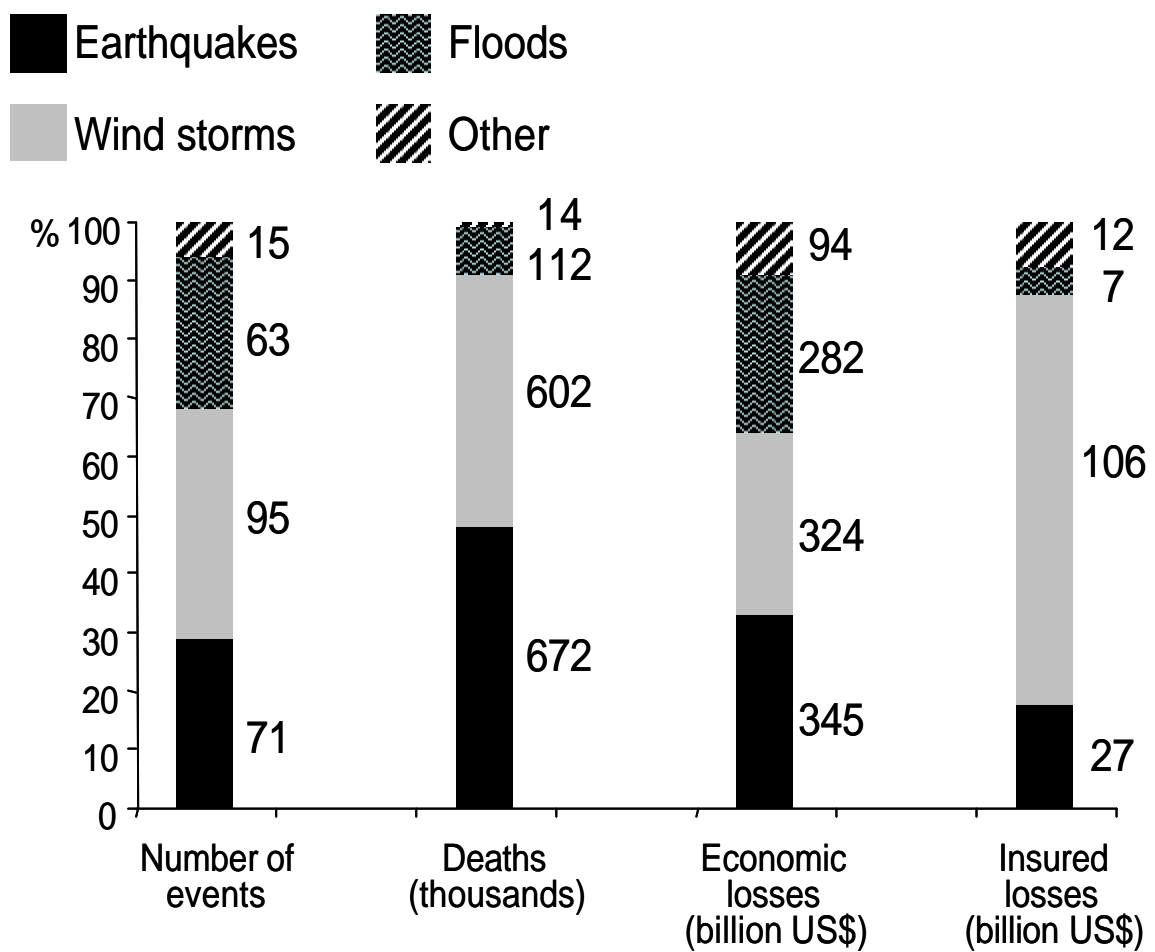


Figure 1

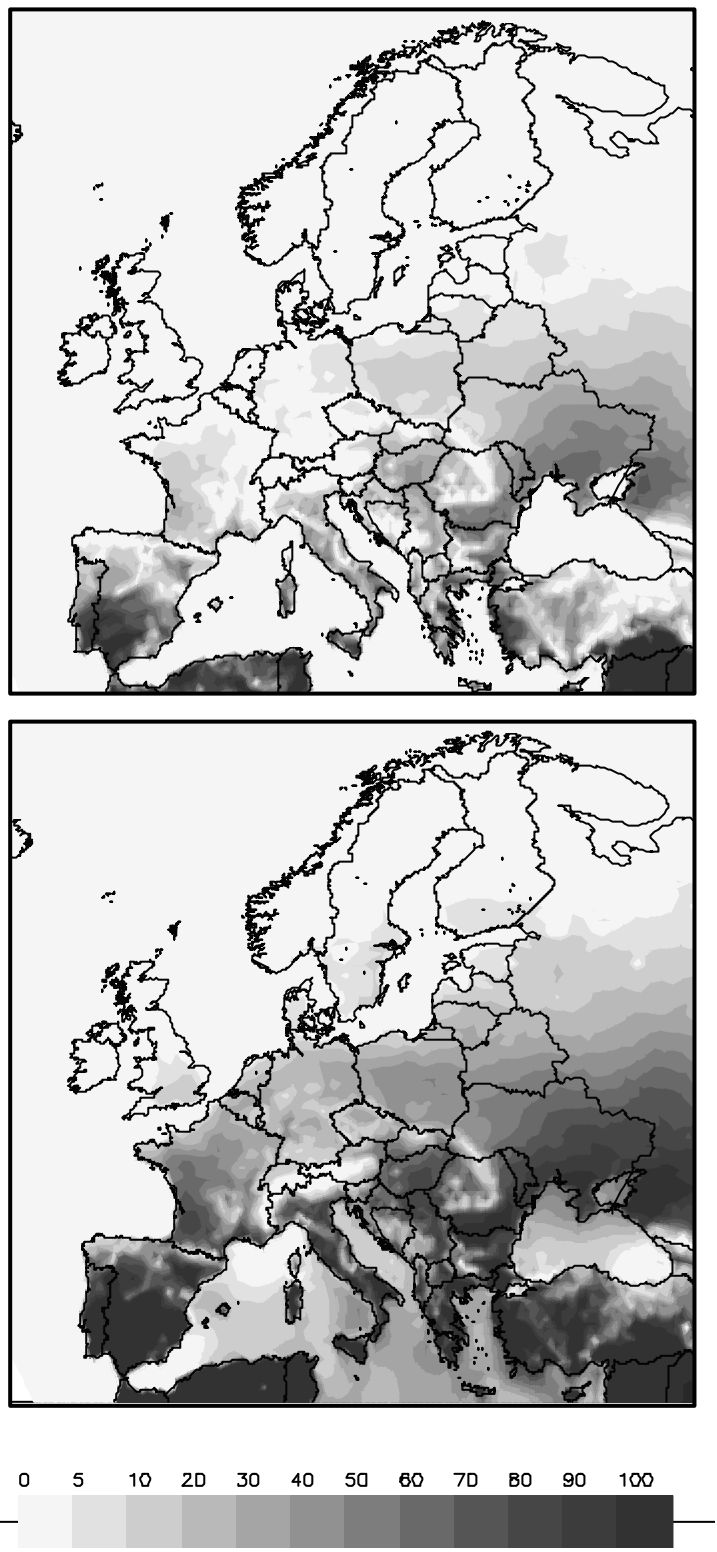


Figure 2

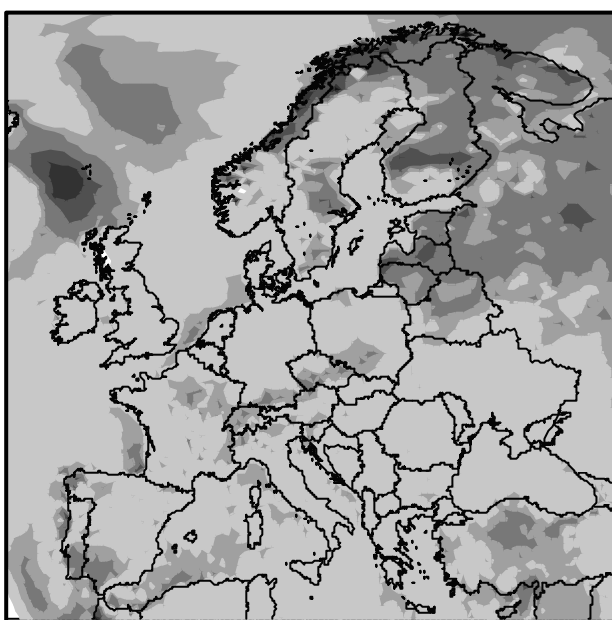
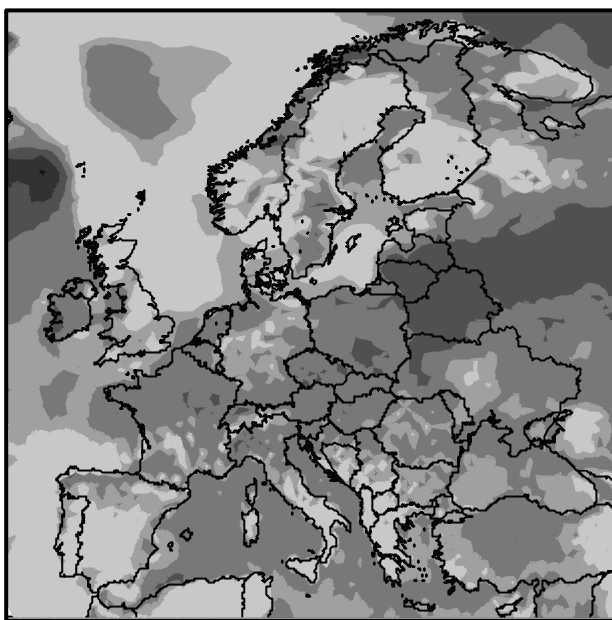


Figure 3

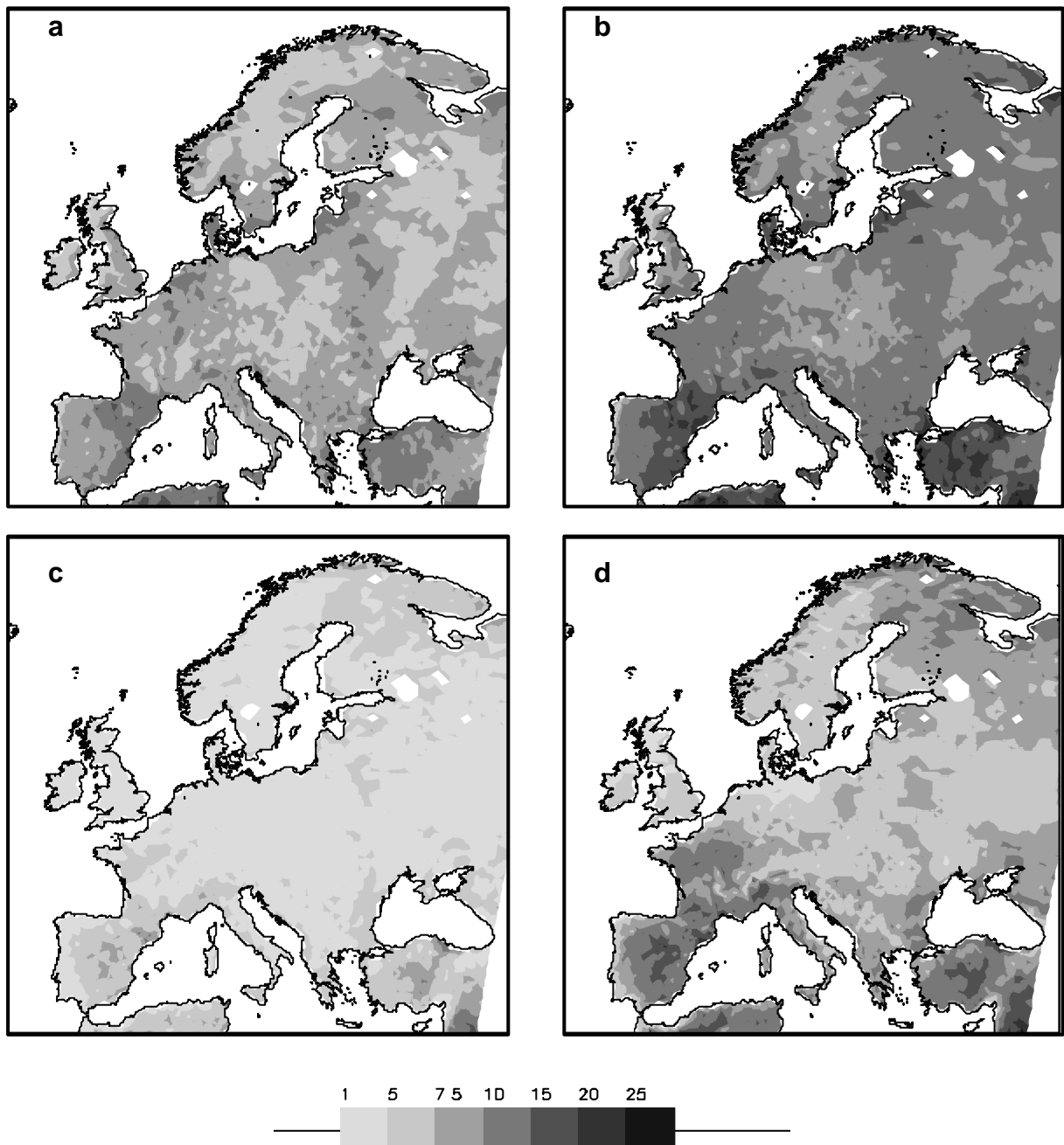


Figure 4

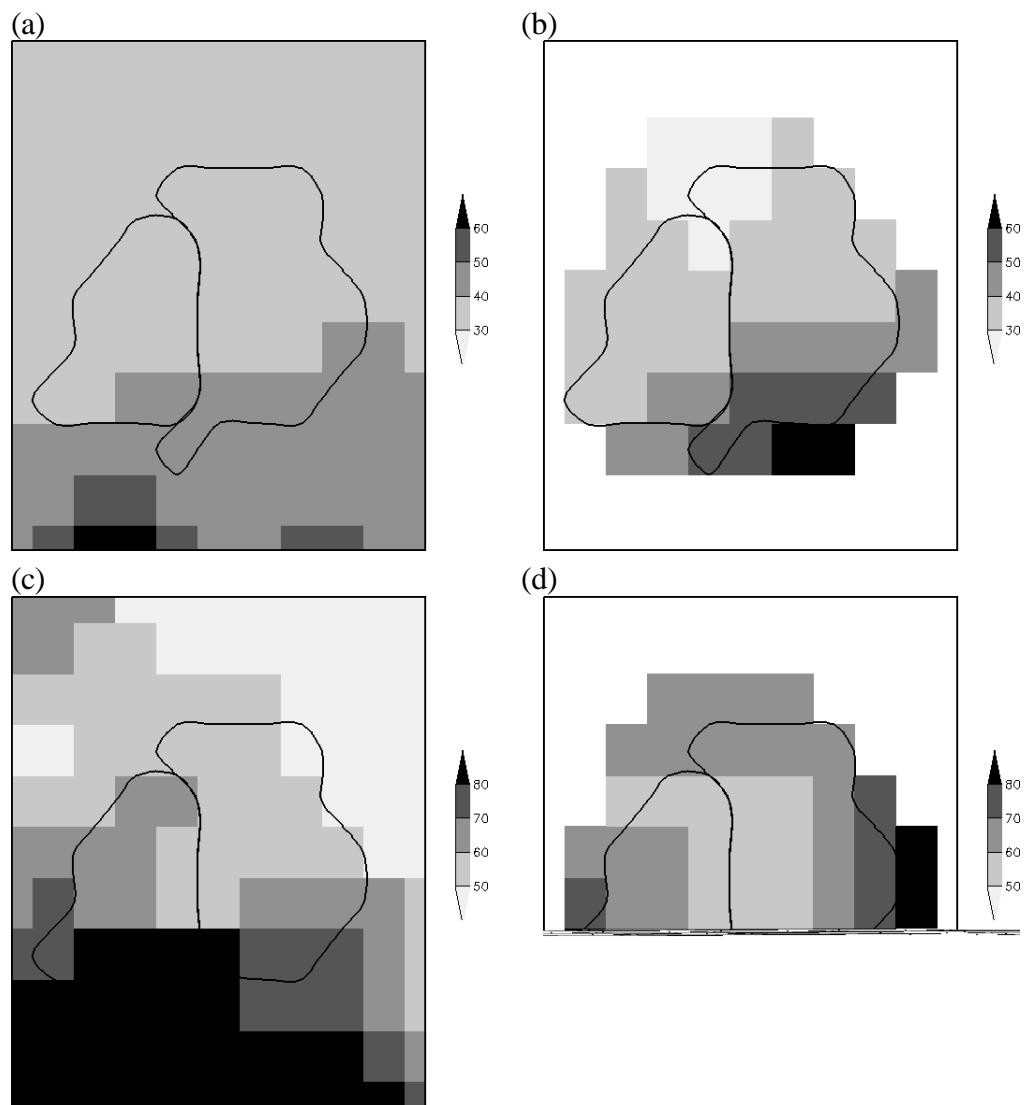


Figure 5

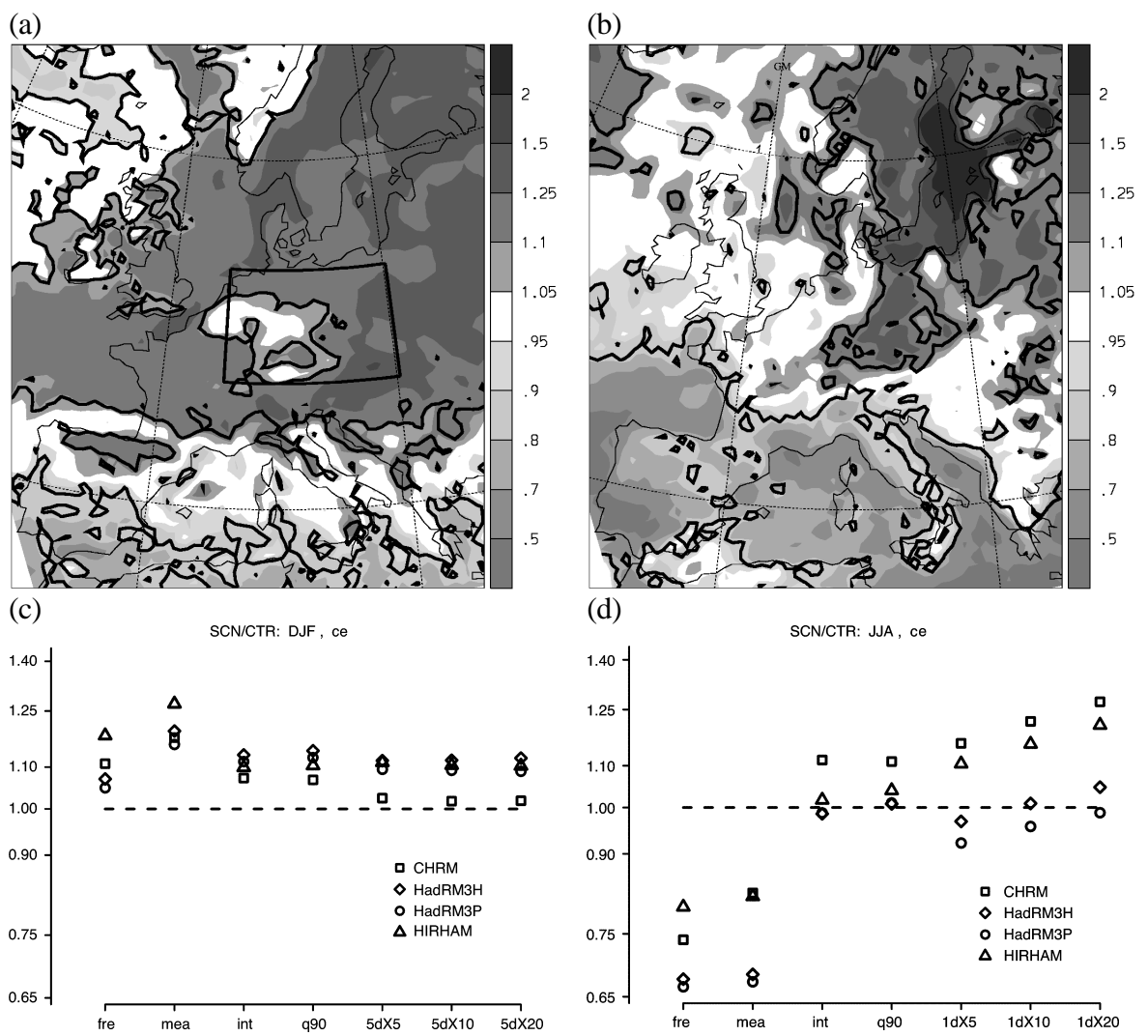


Figure 6

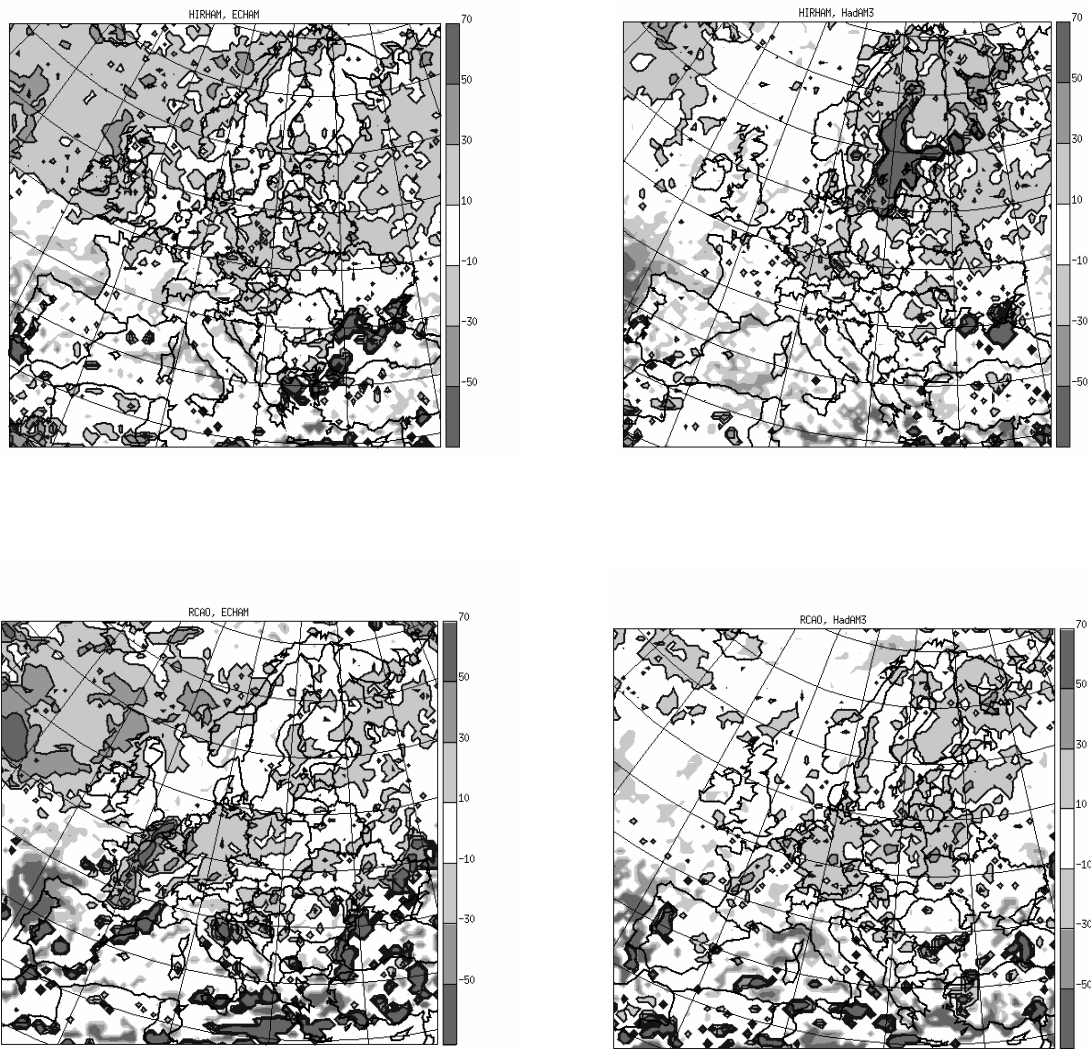


Figure 7 (a : Upper left ; b : Upper right ; c : Lower left ; d : Lower right)

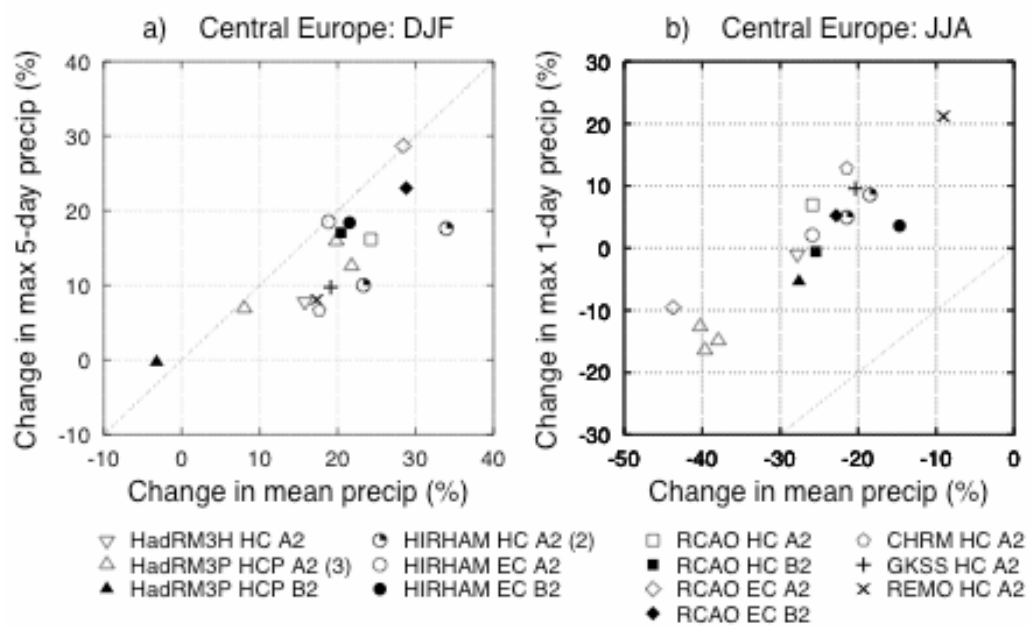


Figure 8

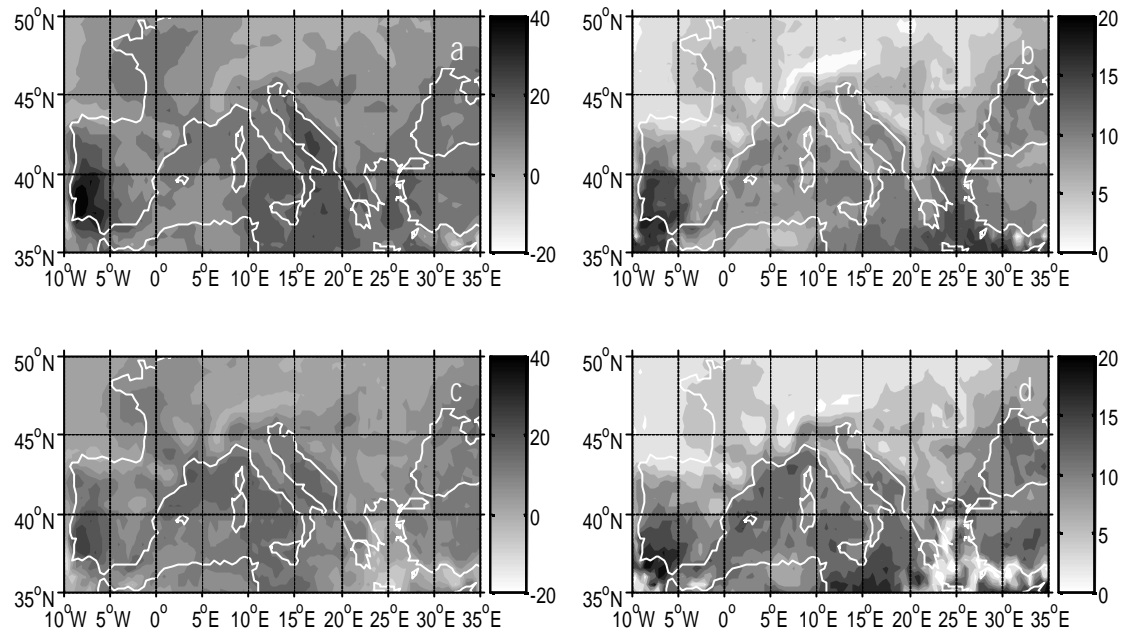


Figure 9: a) A2a: Maximum dry spells (days); b) A2a confidence range (days); c) B2a: Maximum dry spells (days); d) B2a confidence range (days)

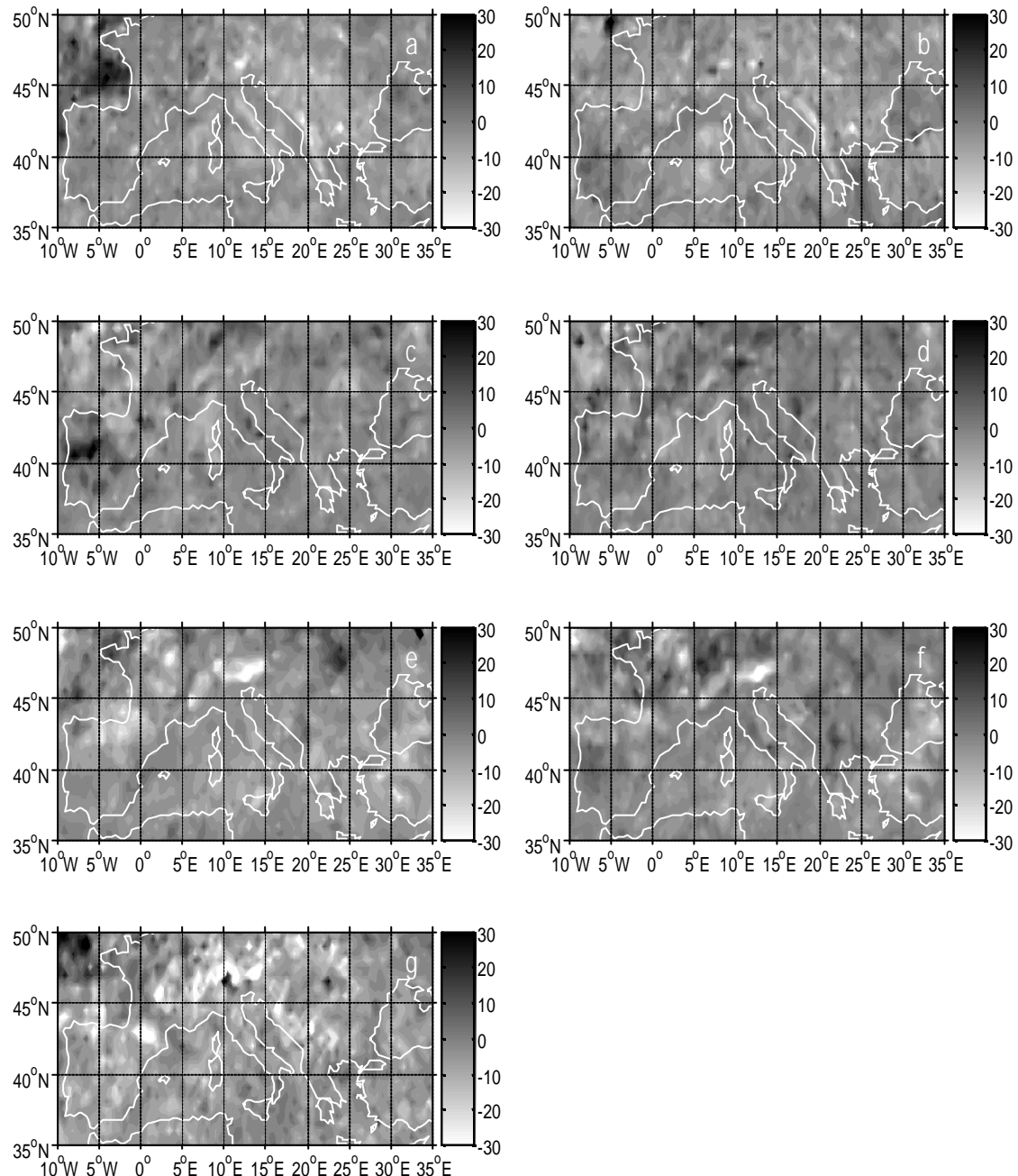
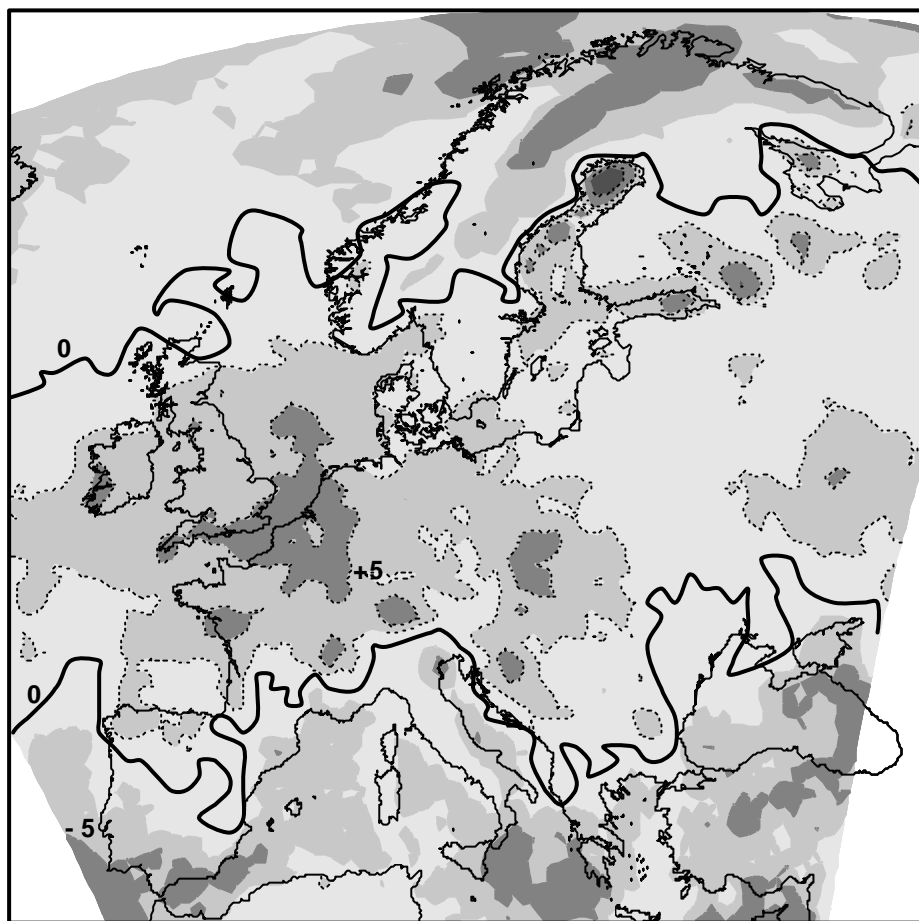


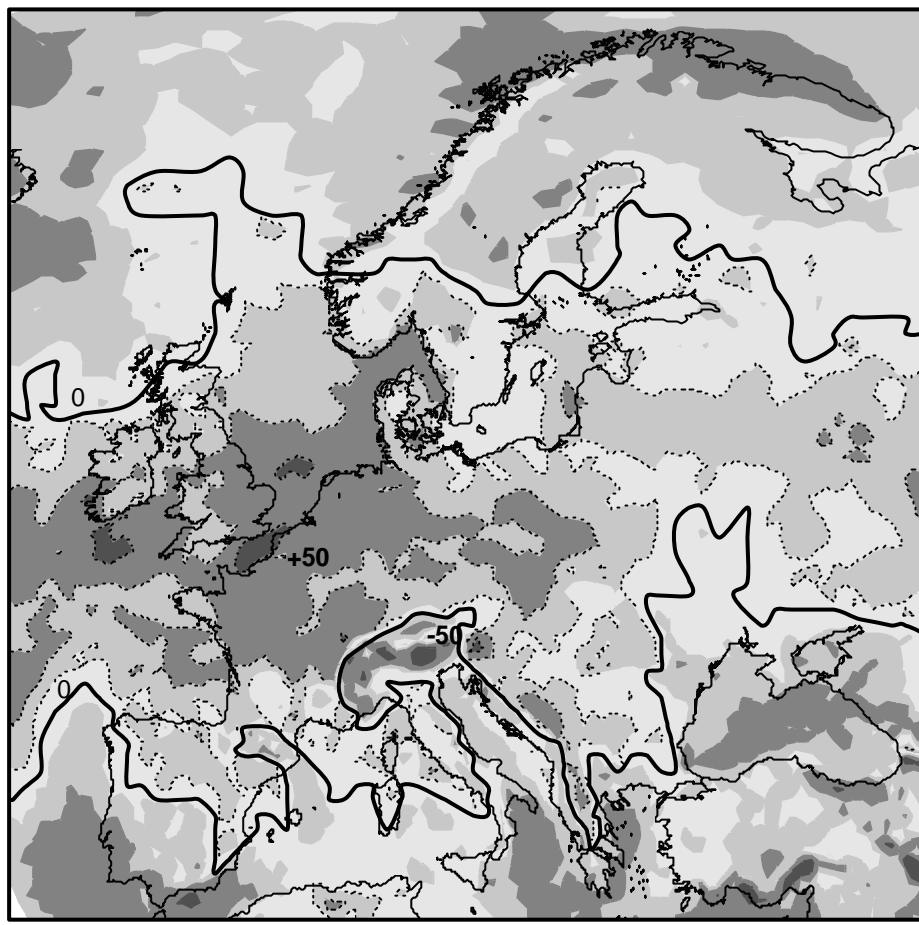
Figure 10: 100-year return levels of maximum length of wet spells for the following models: a) HadRM3P A2a; b) HadRM3P B2a; c) SMHI-HC A2a; d) SMHI-HC B2a; e) SMHI-MPI A2a; f) SMHI-MPI B2a; g) DMI A2a



-20 -10 -5 -2.5 +2.5 +5 +10 +20



Figure 11



-100 -50 -25 -10 +10 +25 +50 +100



Figure 12

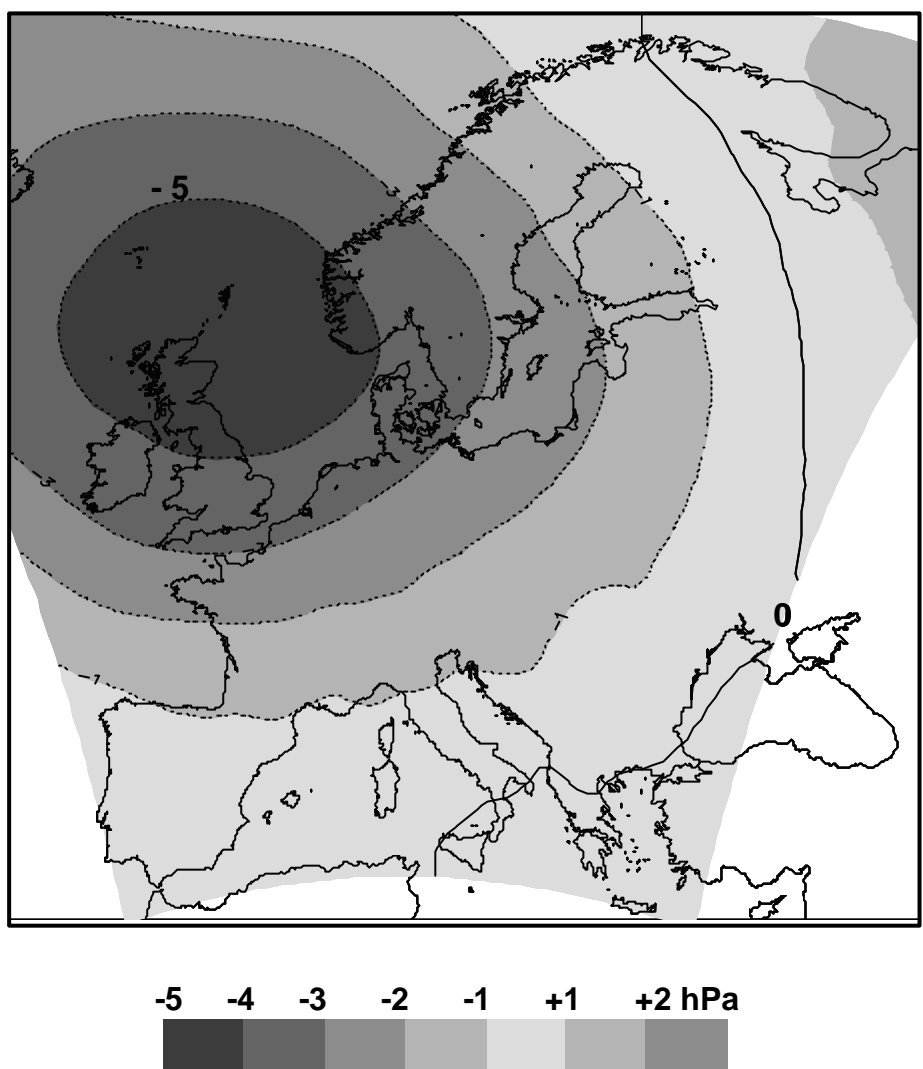


Figure 13

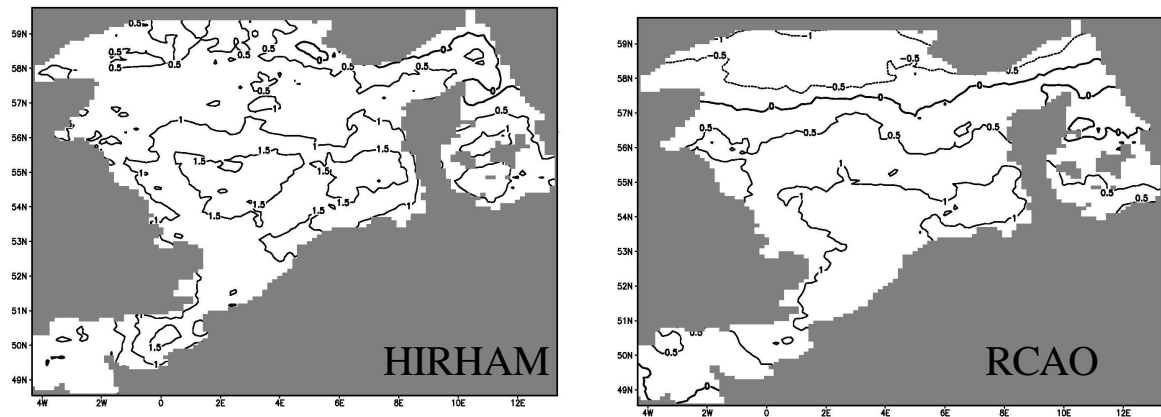


Figure 14

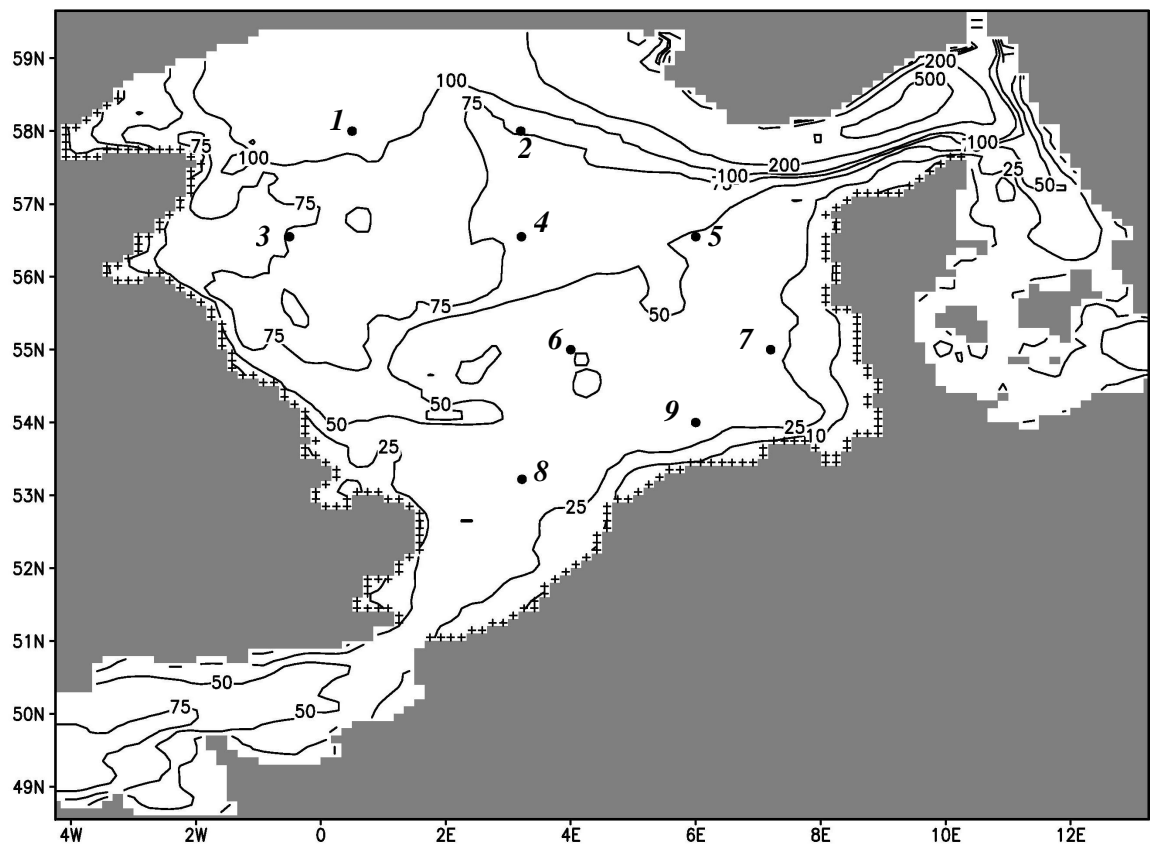


Figure 15

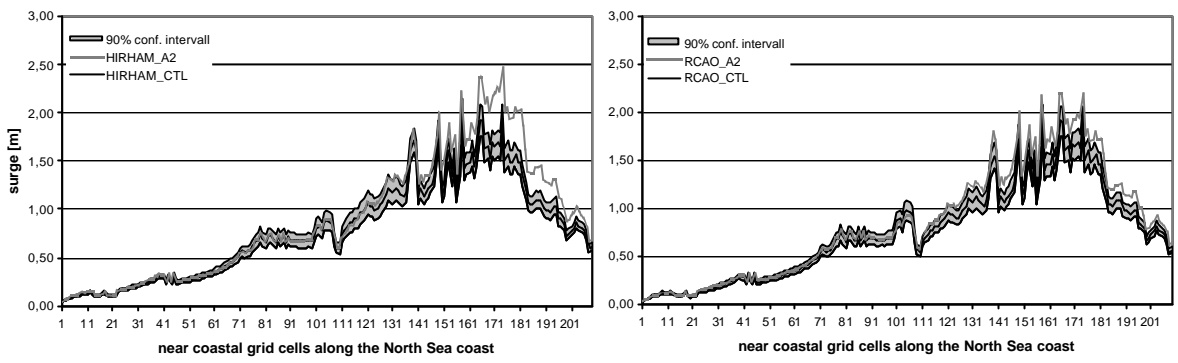


Figure 16